DEVELOPMENT OF A LATERAL MIGRATION RADIOGRAPHY IMAGE GENERATION AND OBJECT RECOGNITION SYSTEM

By

JOSEPH CORNELIS WEHLBURG

A DISSERTATION PRESENTED TO THE GRADUATE SCHOOL
OF THE UNIVERSITY OF FLORIDA IN PARTIAL FULFILLMENT
OF THE REQUIREMENTS FOR THE DEGREE OF
DOCTOR OF PHILOSOPHY

UNIVERSITY OF FLORIDA

1997

This dissertation is dedicated to my parents Dr. and Mrs. Wehlburg, my wife Christine and my daughter Rachel.

ACKNOWLEDGMENTS

The author expresses his appreciation for the guidance and financial support provided by his academic advisor, Dr. Alan Jacobs. The author is additionally indebted to the rest of his Ph.D. committee, Dr. Edward Dugan, Dr. Samim Anghaie, Dr. Andrew Laine and Dr. Martin Vala for the support and encouragement. The author would also like to thank Dan Ekdahl for all his help with the electronics The author thanks the U.S. Army CECOM Night Vision and Electronic Sensor Directorate for providing financial support for conducting this research.

The author expresses special thanks to Dr. Shyam Keshavmurthy for all the help that he gave during the course of the project.

Finally, the author would like to acknowledge that this dissertation would not have been completed without his wife, Christine, and all her editorial guidance, understanding and support.

TABLE OF CONTENTS

page

ACKNOWLEDGMENTS....iii

ABSTRACT....vi

CHAPTERS

1 INTRODUCTION....1

2 CONFIGURATION FOR THE LATERAL MIGRATION RADIOGRAPHY SYSTEM....6

The X-ray Machine....6
The Soilbox....10
The Motion Control and Data Acquisition System....10
The Detector System....13
Previous Detector Designs....13
New Detector Design....16
Detector Size Variation....18
Current Detector Configuration....22
Signal Processing....22

3 RESULTS AND DISCUSSION....26

Image Processing....26
Filtering....26
Surface Feature Identification....26
Buried Feature Identification....32
Depth of Burial....37
Detector Height Variations....40
Surface Variations....47
Resolution Improvement....50
Pattern Recognition....57

4 CONCLUSIONS....67

APPENDICES

A CODE FOR THE MOTION CONTROL AND DATA ACQUISITION SYSTEM....72

B SURFACE FEATURE DETECTION CODE....78

C BURIED FEATURE DETECTION CODE....85

D PATTERN RECOGNITION CODE....93

LIST OF REFERENCES....96

BIOGRAPHICAL SKETCH....98

Abstract of Dissertation Presented to the Graduate School
of the University of Florida in Partial Fulfillment of the
Requirements for the Degree of Doctor of Philosophy

DEVELOPMENT OF A LATERAL MIGRATION RADIOGRAPHY IMAGE GENERATION AND OBJECT RECOGNITION SYSTEM

By

Joseph Cornelis Wehlburg

May 1997

Chairman: Alan M. Jacobs
Major Department: Nuclear and Radiological Engineering Sciences

Compton Backscatter Imaging (CBI) has always been impeded by inefficient sensing of information carrying photons, and extensive structured noise due to object surface features and heterogeneity. In this research project, a new variant of CBI, which substantially resolves both impediments, is suggested, developed and rigorously tested by application to a difficult imaging problem. The new approach is termed Lateral Migration Radiography (LMR) which aptly describes the specific photon history process giving rise to resulting image contrast.

The photons employed in this research are conventionally generated x rays. A pencil x-ray beam with a typical filtered-bremsstrahlung photon energy spectrum is perpendicularly incident upon, and systematically rastered over, the object to be imaged. Efficient sensing of information-carrying photons is achieved by employing large-area detectors with sensitive planes perpendicular to the incident beam. A geometric array of a group of such detectors along with varying degrees of detector collimation to discriminate singly-scattered from multiple-scattered, detected x rays is developed. The direct output of the detector-array components is algebraically combined to eliminate image cloaking by surface features and heterogeneity. Image contrast is generated by the variation of x-ray interaction probabilities in the internal details relative to the surrounding material. These major improvements to conventional CBI have allowed the detection of internals with clarity such that recognition of the internal features via the image details is possible in cases where ordinary CBI can not even detect the presence of the internal structure.

The test application is the detection and recognition of all-plastic antitank landmines buried in soil at depths of up to three inches. In the military application of clearing 12 inch diameter mines from 14-foot-wide tank-lanes, the spatial resolution requirement of one inch and the speed of 3 to 5 mph over rough terrain and cluttered soil surfaces presents a formidable detection and recognition problem. This application requires special x-ray generators, which are under development elsewhere. This research project clearly demonstrates that, given a satisfactory x-ray generator, LMR provides a viable landmine image formation and recognition technique. Potential application of the new LMR technique to general non-destructive inspection (NDI) problems are also discussed.

CHAPTER 1
INTRODUCTION

Lateral Migration Radiography (LMR)[1,2,3,4,5] is a form of Compton Backscatter Imaging (CBI). Compton scattering occurs when a photon interacts with an electron and transfers energy to the electron by kinematic laws.[6] For the materials that are of interest for the example studied, landmine detection, the Compton effect dominates. The backscatter modality has the advantage of not requiring a detector behind the object being imaged, allowing non-intrusive imaging. Some currently marketed systems that employ the backscatter modality are Compton x-ray backscatter inspection system (ComScan)[7] and Dynamic Radiography.[8]

One of the limits of CBI systems is inefficient detection of information carrying photons. The detection ability of CBI systems is also impaired by the presence of surface features and heterogeneity which cause structured noise to appear in the images. This research focused on developing a system which would remove many of the limitations from the CBI system. The problems inherent in CBI systems that were addressed are: separation of surface and subsurface features, detection efficiency, and detector-to-target distance variations (detector height variation). Other topics that were investigated during this research are: image resolution, detector design, and pattern recognition.

Lateral migration for this project is the motion of photons transverse to the incident beam through objects. Photons that undergo lateral migration and are detected must experience more than one collision. In order to detect photons that undergo lateral migration, collimated detectors must be used. The collimators prevent photons that have only undergone one collision from reaching the detectors shielded by the collimators. Conventional CBI systems used only two collimated detectors.[9] Since photons that have experienced lateral migrations contain information about objects below the surface it seems that only collimated detectors would be required to identify subsurface features. The problem with this conclusion is the photon's path is influenced by surface features the photon passed through. This means that the collimated detectors' response contains information about the surface of an object mixed in with the subsurface information. In order to separate surface from subsurface feature information, uncollimated detectors were added. Photons that hit the surface and scatter back can be efficiently detected by an uncollimated detector placed near the x-ray source. This combination of collimated and uncollimated detectors allows subsurface objects to be separated from surface objects.

In the energy range of 10 keV to 10 MeV there are three possible photon interactions: Compton scatter (incoherent scatter), the photoelectric effect, and pair production.[6] The energy range in which the LMR system operates, when applied to the problem that was used to evaluate it, landmine detection, is well below the 1.02 MeV that is required for pair production. This makes the only interactions of interest for this application Compton scattering and the photoelectric effect.

The LMR system responds to changes in the Compton scattering cross section (σ_s) and the photoelectric effect cross section (σ_a) in the target medium. To identify the behavior of the LMR system all the photons created by interactions must be accounted for, even ones that occur after the primary effects of the interaction. After a photoelectric interaction a photon is emitted when an electron is absorbed back into the created vacancy (phosphorescence). The phosphorescence photon has a very small probability of reaching the detector, so the photoelectric effect acts as an absorption process for LMR systems. Table 1 gives a list of phosphorescence (K-edge) energies for some elements that are of interest to the landmine detection system. Typical energies that can reach the detector are on the order of 20 keV or greater for the current system as applied to landmine detection.

Table 1. Phosphorescence energy for some of the elements of interest in landmine detection

Element	H	C	N	O	Si	Fe
Z	1.00	6.00	7.00	8.00	14.00	26.00
K-edge energy keV	0.01	0.28	0.40	0.53	1.84	7.11

Source: Attix[10]

Lateral migration occurs in all objects, surface or buried, high or low σ_s/σ_a. Lateral migration only plays a significant role when materials have a reasonably different σ_s/σ_a relative to the surrounding media and are imaged with collimated detectors. An object with a high σ_s/σ_a allows more photons to survive if they travel through the object instead of through the surrounding media. The migration effect yields an increase in the collimated detector response when the source is over a buried object that allows the photon to have a greater distance of travel in the object than in the surrounding medium.

Table 2 shows calculated Monte Carlo n-particle (MCNP) simulation results for the energy deposition of different collision components for the collimated detectors.

Table 2. MCNP calculated energy deposition by collision component for the collimated detectors.

Energy deposited by collision component (MeV/gm per source x-ray) [4.8% uncertainty in total energy deposition]				
1.00	2.00	3.00	4.00	All
$2.06\text{x}10^{-10}$ (12.0%)	$4.22\text{x}10^{-10}$ (24.7%)	$3.74\text{x}10^{-10}$ (21.9%)	$4.17\text{x}10^{-10}$ (24.4%)	$1.70\text{x}10^{-9}$

Source: Keshavmurthy[11]

Table 3 shows MCNP calculated results for the energy deposition of different collision components for the uncollimated detectors. These MCNP calculations showed that the collimated detectors receive ~90% of their energy deposition from x rays with more than one interaction and ~75% of the energy deposition in the uncollimated detectors results from x rays with only one or two interactions. The MCNP calculations agree with the experimental conclusions deduced from the collimated and uncollimated detector responses.

Table 3. MCNP calculated energy deposition by collision component for the uncollimated detectors.

Energy deposited by collision component (MeV/gm per source x-ray) [1.6% uncertainty in total energy deposition]				
1.00	2.00	3.00	4.00	All
$2.94\text{x}10^{-8}$ (55.3%)	$1.15\text{x}10^{-8}$ (21.6%)	$6.04\text{x}10^{-9}$ (11.4%)	$2.97\text{x}10^{-9}$ (5.6%)	$5.32\text{x}10^{-8}$

Source: Keshavmurthy[11]

Since the uncollimated detectors respond primarily to surface features, caused by the dominance of the lower-order scattering energy deposition, the uncollimated detector response could now be used to separate the surface and subsurface features from the collimated detectors' response. Consequently, the change from the two detector system to the four detector system required the development of an image processing algorithm that could separate surface and buried features. As an example of possible applications for the LMR system, landmine detection was investigated. Additional features required for a landmine detection system are the capability to detect both metal and plastic landmines, adjust to changes in detector height and distinguish terrain variations such as potholes.

For the application of landmine detection, adding two more detectors to the system raised concerns about the weight of the apparatus. Saving weight without adding unreasonable expense is a benefit in any mobile system. The collimated detectors utilized in the LMR system weigh 41 lb. each and have an active detector area of 144 in^2. Instead of purchasing the same commercial detectors for the uncollimated detection system, new lighter and smaller detectors were designed and built.

Chapter 2 covers the experimental configuration including data acquisition and detector design. Chapter 3 addresses the image processing used for the LMR system when applied to landmine detection, including surface and subsurface feature detection, and provides results and discussion regarding detector height variations, terrain variations and resolution improvement. Chapter 4 discusses the overall accomplishments and limitations of the LMR system and provides suggestions for future work.

CHAPTER 2

CONFIGURATION FOR THE LATERAL MIGRATION RADIOGRAPHY SYSTEM

The X-ray Machine

The x-ray machine used at the University of Florida Landmine Detection Facility (UFLMDF) is a Maxitron 300 made by General Electric.[12] It has a maximum output voltage of 300 kV peak (kVp) with an anode current of 20 mA. The Maxitron is considered a continuous photon source with a half-wave rectified output instead of functioning in DC. The photon output has a frequency of 1.2 kHz with a superimposed harmonic of 120 Hz. Figure 1 shows the normalized photon output of the Maxitron 300. Figure 2 shows a schematic of the Maxitron 300 components. The original purpose for the Maxitron 300 was a deep therapy machine for treating cancer patients. In order to configure the machine for use in an LMR system, several changes were required. To shield against stray photons leaking out of the head, extra lead shielding was installed. Low energy (< 10 keV) photons were filtered out with an additional 720 mg/cm^2 Al filter to decrease the surface noise. The photon beam was then recollimated to create a 2 cm x 2 cm spot on the soil. The beam was recollimated to remove the scattered flux caused by the additional Al filter. Figure 3 shows a photograph of the experimental setup with the x-ray machine above the soilbox.

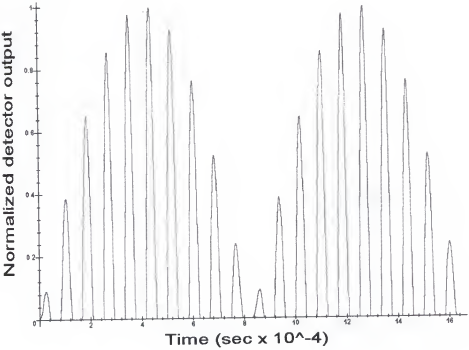

Figure 1. Normalized photon output of the Maxitron 300.

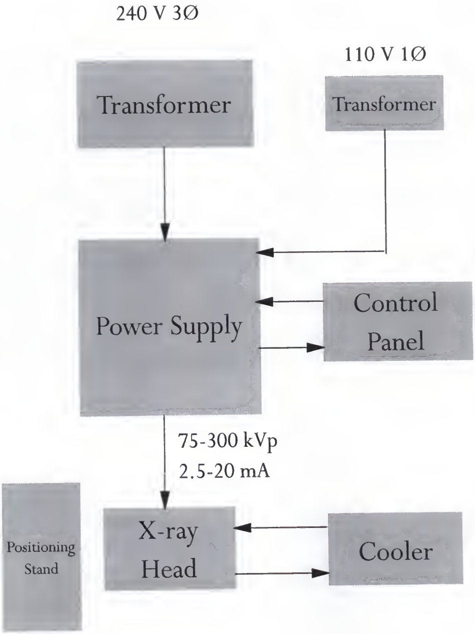

Figure 2. Schematic of the Maxitron 300.

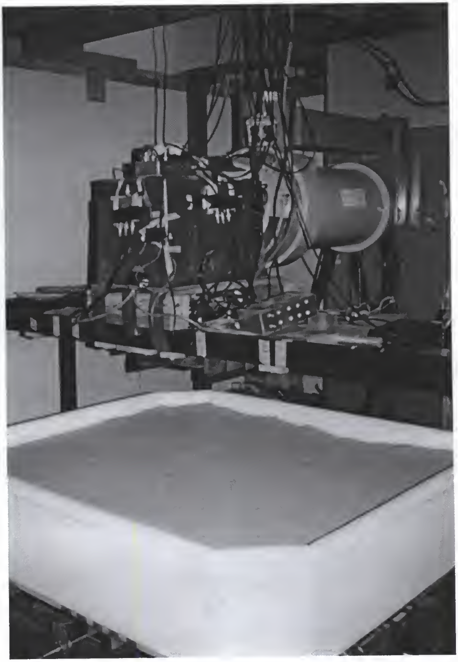

Figure 3. Landmine Detection Experimental Setup.

The Soilbox

The first soilbox at the UFLMDF was built by Moss and had the dimensions 36"x48"x18".[13] The size of the soilbox limited the size of the landmine images to 17"x17" to prevent edge effects caused by the detectors nearing the wooden wall of the soilbox and detecting photons that have scattered off the wall. To allow larger images to be taken, the size of the soilbox was increased to 48"x55.5"x12". The depth of the new soilbox was reduced to limit the increase in weight due to the increase in area. Figure 4 shows the current soilbox and the original for comparison.

The Motion Control and Data Acquisition System

The original motion control and data acquisition system was a GPIB-based system designed by Moss[13] and then modified by Monroe to a data acquisition board system capable of supporting two detectors.[14] The soilbox motion shown in Figure 5, termed bousterphedonic rastering, allows the system to image the ground in a time efficient manner. The refined LMR system uses four detectors, each needing a sampling rate of 50 kHz. Thus, a new motion control and data acquisition system was required.

The new system is controlled by a Pentium-66 computer running National Instrument's LabView 3.1.1. LabView is a graphical programming language that allows real-time data acquisition, signal processing, and motion control. A National Instruments AT-MIO-16F-5 multi-function analog and digital I/O card with a maximum throughput of 200 kHz is utilized so all four detectors could be sampled simultaneously at 50 kHz. The digital I/O on the data acquisition card is used to control the eight motor relays. The

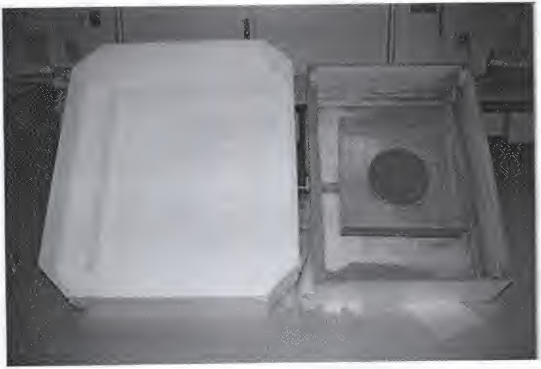

Figure 4. Picture of the current soilbox (left) compared to the original (right).

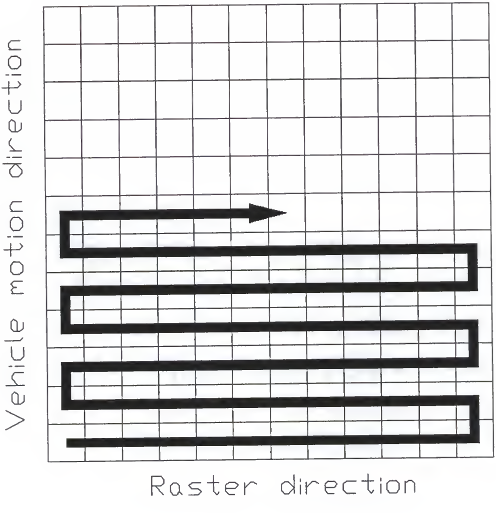

Figure 5. Diagram showing bousterphedonic rastering.

motors require one relay for each direction (forward and reverse), one relay to engage the clutch and one relay to turn off the motor. A National Instruments PC-DIO-24 digital I/O card is used to read the outputs from the two optical encoders that determine the position of the soilbox during image acquisition. The resolution of the optical encoders gives ~5000 divisions per inch which allows fine positioning of the soilbox. Figure 6 shows a block diagram of the data acquisition and motion control system.

The motion control and data acquisition system coordinates sampling of all four detectors, saves the detector data, and determines the direction and duration of each motor motion. The Labview code written to run the system samples all four detector simultaneously, stores the detector response along with the current soilbox position, then based on the soilbox position and the step size, determines which motor needs to be moved, which direction it needs to go and for how long the motor needs to run before sampling the detectors again. Figure 7 shows the control panel for the LMR landmine detection system. Information about the current run is entered into the logfile and the desired number of steps for the image is set. A visual representation of the code is in Appendix A.

The Detector System

Previous Detector Designs

The light sensing element of detectors can operate in two modes. In the voltage mode, the light sensing element responds to an individual quantum of radiation that

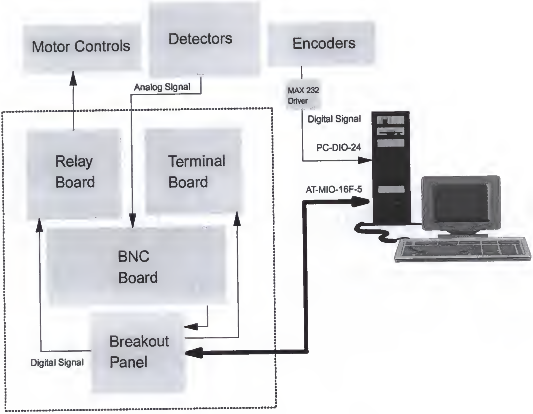

Figure 6. Block diagram of the data acquisition and motion control system.

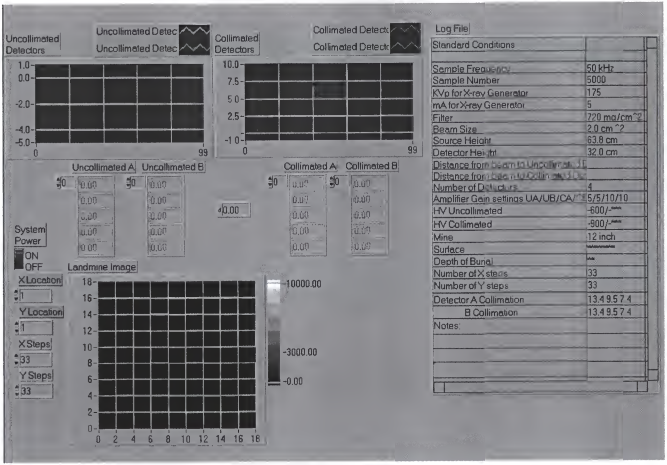

X Location: 1

Y Location: 1

X Steps: 33

Y Steps: 33

Standard Conditions	
Sample Frequency	50 kHz
Sample Number	5000
KVp for X-ray Generator	175
mA for X-ray Generator	5
Filter	720 mg/cm^2
Beam Size	2.0 cm ^2
Source Height	63.8 cm
Detector Height	32.0 cm
Distance from beam to Uncollimated D	
Distance from beam to Collimated D	
Number of Detectors	4
Amplifier Gain settings UA/UB/CA/C	5/5/10/10
HV Uncollimated	-600/-
HV Collimated	-900/-
Mine	12 inch
Surface	
Depth of Burial	
Number of X steps	33
Number of Y steps	33
Detector A Collimation	13.4 9.5 7 4
B Collimation	13.4 9.5 7 4
Notes:	

Figure 7. Data acquisition control panel for landmine detection system.

interacts with the detector. The benefit of this mode is that the detector can provide spectral data from the radiation field. A drawback of this mode is that the detector can suffer from pulse-pileup if the flux is high. In the current mode, the light sensing element responds to the amount of energy being deposited on the detector and allows the detector to operate in high flux fields without pulse-pileup. The disadvantage of operating in current mode is there is no way to gather spectral information about the radiation field.

The backscatter landmine detector project has used a variety of scintillator detector systems with Photomultiplier (PM) tube light sensors. Campbell[15] used two types of scintillators, a terbium-activated, gadolinium oxysulfide, rare earth screen-based scintillator and a sodium iodide based scintillator. Both detectors used PM-tube light sensing elements operated in the voltage mode. Monroe[16] changed to BICRON scintillating detectors that used BC400 as the scintillator. BC400 is a polyvinyltoluene based scintillator made by BICRON for general purpose detectors. Monroe also switched the PM tube light sensor in the BICRON detectors to current mode to prevent pulse-pileup.

New Detector Design

Investigation into a new detector design to be used as the uncollimated detectors resulted in the evaluation of three types of light sensing units; a pin diode, an avalanche photodiode (APD), and a PM-tube. In addition six different scintillating materials were also evaluated: Hi-Plus (HP), Quanta III (Q3), Ultra-Vision Rapid Back (UVRB), Ultra-Vision Super Rapid Back (UVSRB), Quanta Fast Detail (QFD), and Quanta Super

Rapid Back (QSRB). The pin diode and the APD were both made by Advanced Photonix and the PM tube was made by Hamamatsu. The scintillating materials were all made by DuPont and use a rare earth phosphor with a polyester base. The screens are currently marketed by Sterling Diagnostic Imaging, Inc.

The pin-diode was not able to rival the APD or the PM-tube for readily achievable gain without cooling the pin-diode to lower the dark current. The cooling process was determined to be too complex a system for the LMR landmine detection system. The APD has a 0.63 in diameter active area and the bias voltage used for the experiments was 2.5 kV which resulted in a current amplification of ~1000 and a dark current of 2 μA. The need for a high-bias-voltage coupled with the large dark current prompted the search for a better light sensing element. The PM-tube had been considered for the project because the collimated detectors were already using PM-tubes, but they were large and fragile. In 1994 Hamamatsu developed the OPTO-8 PM-tube, which has an 0.32 in diameter active area and overall dimensions of 0.63 in diameter by 0.45 in long. The OPTO-8 was capable of gains of $3\text{x}10^5$ at -800 V bias with a dark current of 2 nA. The increased gain and lowering of bias combined with the reduced dark current made the OPTO-8 the light sensing element of choice for the new detector.

To evaluate the scintillating material a cone-shaped housing was used. The cone is 22.8 in high with a 30° viewing angle and was constructed by Monroe.[14] A Hamamatsu R647 PM-tube (in current mode) was used as the light sensing element. Table 4 shows the results of the scintillator tests. To get the strongest signal out of the new detector, QSRB was chosen as the scintillator.

Table 4. Comparison of DuPont Scintillator Screens.

Screen Type	Peak Voltage Response (Volts)
HP	0.39
Q3	0.79
UVRB	0.25
UVSRB	0.80
QFD	0.53
QSRB	1.34

The body of the new detector housing was designed to optimize the spatial response of the detector to incoming photons. Figure 8 shows pictures of the detector with one of the light sensing elements installed. The detector housing is designed for three light sensing elements. The detector housing is constructed out of 1/16" brass with all the joints soldered together. The plastic scintillator is mounted on the bottom of the detector housing and was protected by 1/32" Al sheet. The active area of the new detector is 48 in^2 (4 in by 12 in).

Detector Size Variation

The BICRON collimated detectors weigh 41 lb. each and have an active detector area of 144 in^2 (12 in by 12 in). To investigate how efficiently the system uses the area of the collimated detectors, portions of one of the collimated detectors was covered with 1/8" lead sheeting and compared to the uncovered detector response. Table 5 shows the

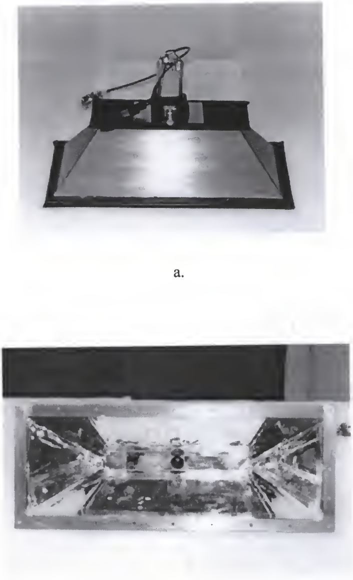

a.

b.

Figure 8. Pictures of the new detector design.
a. Side view of the new detector. b. View of the inside of the new detector.

Table 5. Collimated BICRON Detector Spatial Response.

Measurements Number	Shielded Fraction		
	Uncovered	Outer 1/3	Outer 2/3
1	21,933.00	18,190.00	14,593.00
2	21,459.00	17,994.00	14,282.00
3	22,288.00	18,203.00	13,936.00
4	22,183.00	17,557.00	13,955.00
5	21,782.00	18,125.00	14,137.00
6	22,591.00	18,282.00	15,426.00
7	21,719.00	18,838.00	14,589.00
8	22,560.00	17,740.00	14,474.00
9	22,176.00	18,218.00	14,753.00
10	22,246.00	17,820.00	14,001.00
Average	22,093.70	18,096.70	14,414.60

results of the experiment. The collimators used for this experiment were located at the inner edge of the detector ant at 4" and 8" from the inner edge. The lengths were 5.27 in, 3.74 in, and 2.91 in respectively. The results of this test were surprising since it showed that more signal was generated in the outer 1/3 of the detector than in the middle 1/3. The reason for the result is that even though the light pipe for the BICRON detector is good, the outer third of the detector is more sensitive then the middle or the inner third of the detector because of the light pipe design. The conclusion from this test was that the inner 1/3 of the detector accounts for ~2/3 of the detector response.

Consequently, the new detector (active area 48 in^2) was placed in the position typically occupied by the forward BICRON collimated detector. A 5.4" collimator was attached to the new detector and Figure 9 shows the image generated for a 12" mine at location (16,16) and Depth of Burial (DOB) =1". Figure 10 shows the detector response

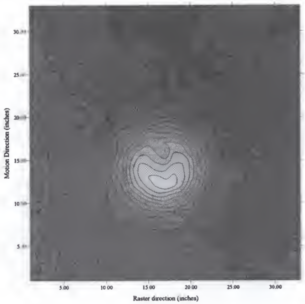

Figure 9. LMR image generated using one of the new uncollimated QSRB scintillator detectors as a collimated detector.

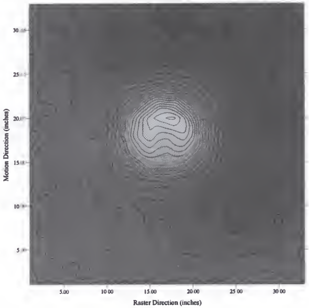

Figure 10. LMR image generated using the standard BICRON collimated detector.

for the rear BICRON collimated detector for the same run as a control example. The benefit of going to the new detector design is that the new 48 in^2 detectors only weigh 7.5 lb. which is a savings of 33.5 lb. (82%) compared to the 144 in^2 BICRON detectors. Assuming a 48 in^2 BICRON detector would weigh 1/3 as much as a 144 in^2 BICRON detector, the weight saved would be ~6.2 lb. (45%).

Current Detector Configuration

The LMR detector system is designed with four detectors. There are two uncollimated detectors using the new detector design and two collimated detectors using the BICRON detectors from the previous CBR system. Figure 11 shows the detector array configuration. The collimators lengths were determined using geometric calculations as shown in Figure 12. The height of the detector above the ground plus the expected DOB of the landmines is (a), the distance from the x-ray beam to the rear of the sensitive area is (b), the width of the sensitive area is (d), and the length of the collimator is (c). Using the principle of similar triangles if a, b, and d are known then c can be determined. The lengths were confirmed using Monte Carlo simulations done by Keshavmurthy.[11]

Signal Processing

The signals coming from the BICRON collimated detectors contain noise suspected to be caused by cosmic radiation which creates a high frequency (> 10 kHz) signal component in the BICRON response. Since the cosmic radiation produces a single

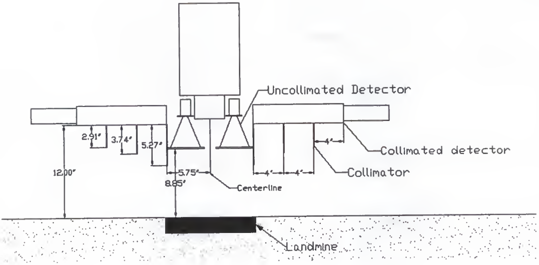

Figure 11. Current four detector system.

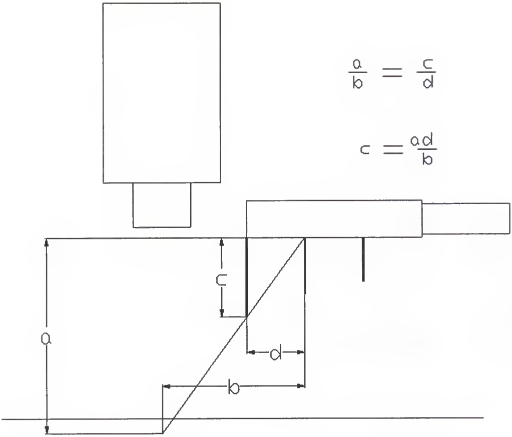

Figure 12. Geometric calculations used to calculate the collimator lengths.

event the apparent bandwidth of the signal is actually just the fastest that the detector and amplifier system can respond. The bandwidth of the amplifiers for the detectors is 10 kHz, so the cosmic radiation pulses are integrated into ~10 kHz high energy peaks. Since the bandwidth of the x-ray signals is 1.2 kHz, the minimum sampling rate (Nyquist limit is equal to two times the bandwidth) would be 2.4 kHz. The Nyquist sampling criteria are for ideal data and it is necessary to sample at 4 to 5 times the bandwidth. Since the amplifier system has some excess bandwidth, the BICRON detector signals are run though a lowpass Chebyshev filter with a cutoff frequency of 5 kHz which removes the unwanted high frequency noise. The new uncollimated detectors are thin screen detectors and did not suffer from the effects of the cosmic radiation.

CHAPTER 3
RESULTS AND DISCUSSION

Image Processing

Filtering

The algorithms developed for the LMR landmine detection system allow the use of a lowpass spatial filter to smooth the image. Figure 13 shows the spatial lowpass filter. Figure 14 shows a sample application of the LMR system, the original rear collimated detector image of a 12" plastic anti-tank mine with a DOB=3". The result of applying the spatial lowpass filter to the image in Figure 14 is shown in Figure 15. Figures 14 and 15 show how the lowpass spatial filter removes statistical noise and variations caused by small surface irregularities. One drawback of using a lowpass spatial filter is that if the objects of interest are small (< 3 pixels) the 3x3 spatial lowpass filter smoothes them away. For the detection of anti-vehicle mines (6 in to 12 in diameter) with the current 1" pixel size the filter is very useful.

Surface Feature Identification

The uncollimated detectors' responses are dominated by surface features, so the use of a dual level segmentation algorithm separates the surface features into scattering and absorbing objects. The surface feature identification code (surfdet.pro) is the implementation of the algorithm in Interactive Data Language (IDL) (see Appendix B).

	i-1	i	i+1
j+1	1.00	1.00	1.00
j	1.00	1.00	1.00
j-1	1.00	1.00	1.00

Figure 13. Spatial lowpass filter matrix.

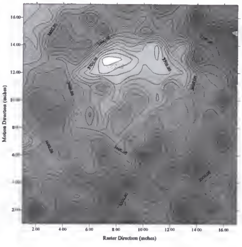

Figure 14. Rear collimated detector image of a 12" plastic anti-tank landmine DOB=3".

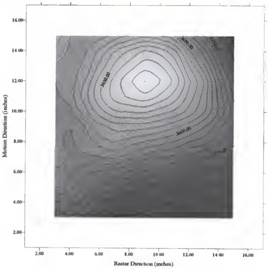

Figure 15. Spatially filtered detector image.

The code determines which objects have a higher σ_s/σ_a and which objects have a lower σ_s/σ_a than the surrounding soil, resolves the location of each object, calculates the x-axis and y-axis dimensions, and computes the size of each object.

A block diagram of the code is shown in Figure 16. The code initially performs spatial lowpass filter on the sum of the uncollimated detector responses as described in the previous section. The signals are then normalized to 256 to facilitate the typical 8-bit resolution used in gray scale images. After normalization, the average pixel value for the image is calculated. Based on the average pixel value for the image, the user is prompted to enter an upper and a lower limit for a pixel of interest. This results in image segmentation. If a pixel contains a value that is above the upper limit, then the pixel is marked as an object with a σ_s/σ_a higher than the surrounding soil. If the pixel value is lower than the lower limit, it is marked as an object with a lower σ_s/σ_a than the surrounding soil.

After the image is segmented, the code uses a 4-connectivity criteria described in Figure 17 to determine if the pixel is part of a glob (object). Globbing removes individual pixels that are too small to be considered important features. Following the globbing routine, each glob is analyzed to determine if it is above a user defined minimum size. The minimum size can be based on the minimum size of the expected objects. If the glob is above the minimum size, the location, x-axis and y-axis dimensions, and size of the glob are determined.

Figure 18 shows input and output for the surface feature detection code when applied to the case of landmine detection, the upper limit was 110% of the average and

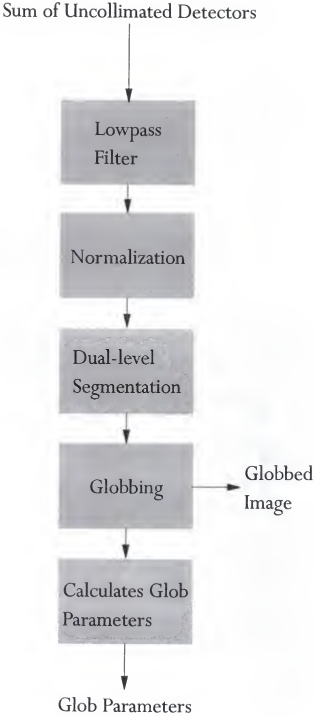

Figure 16. Flow diagram of the surface feature detection code.

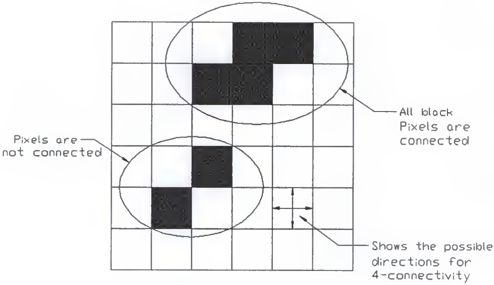

Figure 17. Four connectivity model.

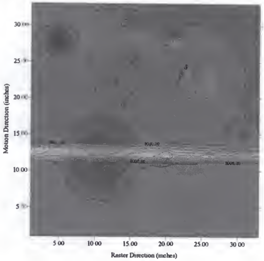

Input

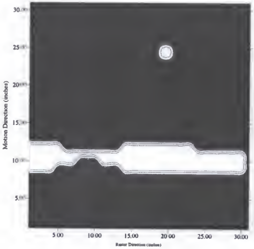

Output

Figure 18. Input and output for the surface feature detection algorithm.

the lower limit was 99% of the average. The input was the uncollimated detector image of a simulated minefield with a 3" diameter metal antipersonnel mine at (4,27), a 12" diameter metal anti-tank mine at (10,10), a 12" diameter plastic anti-tank mine at (23,23), a 2"x2"x36" wooden rod at y=12, and a 2" diameter rock at (21,27) (all mines were buried (DOB) at 1"). The uncollimated image shows primarily the surface features. Table 6 gives the results calculated by the code for the two surface features. Object 1 is the rock at (20,27) and Object 2 is the wooden rod at y=12. The 1" resolution of the system limited the code's ability to locate the center of the rock. The wooden rod was located, but because it is only 2" wide the calculated area and the location were off due to the resolution limit imposed by the 1" pixels .

Table 6. Comparison of Code Results to Actual Values.

Parameters	Actual (in.)	Calculated (in.)	Difference (%)
X_0 object 1	20.00	19.00	-5.00
Y_0 object 1	27.00	24.00	-11.11
Area object 1	4.00	4.00	0.00
X_0 object 2	16.00	15.00	-6.25
Y_0 object 2	12.00	10.00	-16.67
Area object 2	66.00	93.00	40.91

Buried Feature Identification

Since the uncollimated detectors respond primarily to surface features and the collimated detectors responded to both buried and surface features, a method of buried feature identification is possible. Using the surface feature information from the uncollimated detectors the surface feature information in the collimated detectors can be removed by subtraction. A block diagram of the code is shown in Figure 19. The code begins with the same spatial smoothing option as the surface feature detection code. The next step is to normalize the detector images. Next the uncollimated detector response is subtracted from the collimated detector response with the following equation

$$\text{No surface feature image} = \text{norm} \times 255 \times \frac{\text{col(i,j)-cmin}}{\text{cdiff}} - 255 \times \frac{\text{uncol(i,j)-umin}}{\text{udiff}}, \qquad (1)$$

where *col(i,j)* is the collimated detector pixel value at i,j, *uncol(i,j)* is the uncollimated detector pixel value at i,j, *cdiff* is the difference between the maximum and the minimum pixel value for the collimated detector, *udiff* is the difference between the maximum and the minimum pixel value for the uncollimated detector image, *cmin* is the minimum pixel value for the collimated detector image, *umin* is the minimum pixel value for the uncollimated detector image, norm is *cdiff* / *udiff*, and 255 is used as a normalizing value. The equation is derived by a cross-weighting scheme to arrive at images with equal weighting and reasonable contrast.

After the surface features are removed, the code resembles the surface feature detection code. Table 7 gives the results from the buried feature detection code for the same sample image analyzed by the surface feature identification code. Figure 20 shows the collimated and uncollimated detector responses, the response after surface feature removal and the image which leads to the buried feature identification results. Mine 1 is the 3" diameter metal antipersonnel landmine, Mine 2 is the 12" diameter metal anti-tank landmine and Mine 3 is the 12" diameter plastic anti-tank landmine. The 1"

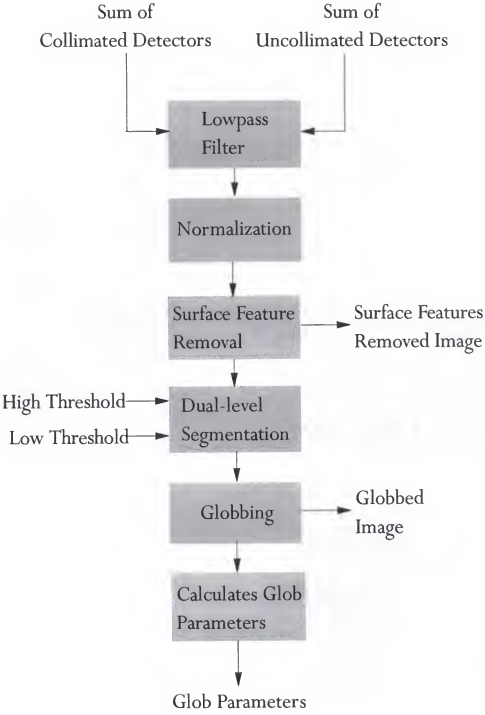

Figure 19. Flow diagram of the buried feature detection code.

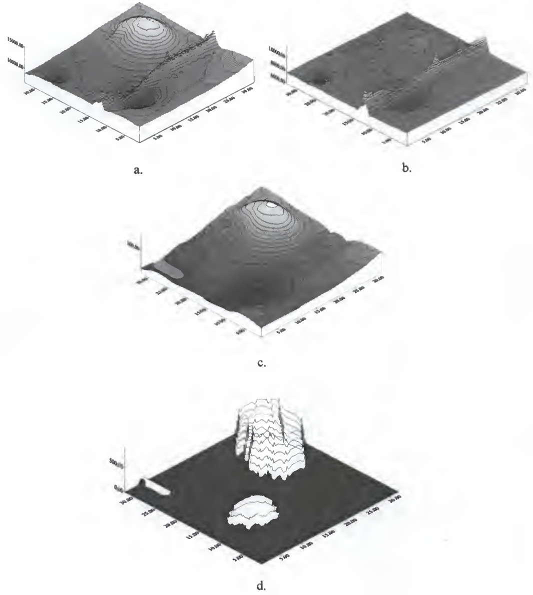

Figure 20. Inputs and outputs for the buried feature detection code. a.) Collimated detector input. b.) Uncollimated detector input. c.) Surface features removed output. d.) Globbed image output

Table 7. Comparison of Code Results to Actual Values.

Parameters	Actual (in)	Calculated (in)	Difference (%)
X_o mine 1	4.00	4.48	12.00
Y_o mine 1	27.00	28.81	6.70
X size mine 1	3.00	5.00	66.67
Y size mine 1	3.00	8.00	166.67
Area mine 1	7.00	31.00	342.86
X_o mine 2	10.00	9.05	-9.50
Y_o mine 2	10.00	11.68	16.80
X size mine 2	12.00	12.00	0.00
Y size mine 2	12.00	8.00	-33.33
Area mine 2	113.00	65.00	-42.48
X_o mine 3	23.00	24.98	8.61
Y_o mine 3	23.00	22.89	-0.48
X size mine 3	12.00	12.00	0.00
Y size mine 3	12.00	14.00	16.67
Area mine 3	113.00	113.00	0.00

resolution of the system did not allow accurate information to be determined about the shape of the 3" landmine due to undersampling. The undersampling error could be corrected by improving the resolution to ~1/2" so that enough data about the object to accurately determine its' size would be obtained. Even with a wooden rod covering Mine 2, the code was able to locate and give a reasonable estimate of the size of the landmine. The rock on Mine 3 did not cause any difficulties in the location of the 12" plastic landmine and all the code's predictions were within 17%. The buried feature detection code is written in FORTRAN 90 and is given in Appendix C.

Depth of Burial

As the DOB of an object increased, the offset between the forward and rear collimated detector images increases. Figure 21 shows the forward and rear detector images for the case of a 12" plastic landmine at (9,9) DOB=0,1", and 2". Table 8 lists the total offset as the DOB was increased.

Table 8. Image offset as a function of DOB.

DOB	0"	1"	2"
Total Offset (in)	4.75	5.00	5.25

Figure 22 gives a visual display of the lateral migration of x-rays through buried objects and demonstrates why the offset occurs in the collimated detectors. In Figure 22a the x-ray beam is at the center of the mine and both detectors respond equally. In Figure 22b the x-ray beam is at the right side of the mine and the left detector signal is greater than the right detector due to the enhanced lateral migration of the x-rays through the landmine. The lateral migration in the landmine is enhanced when the photons spend more time in the landmine where they have a greater change of scattering and a lower chance of absorption then in the surrounding soil. Figure 22c shows how the case is reversed when the x-ray beam is at the left side of the mine. Lateral migration occurs in the landmine in all directions, but the enhanced response is only apparent for migration perpendicular to the collimators because photons that do not scatter perpendicularly to the collimators will be filtered out by the collimators.

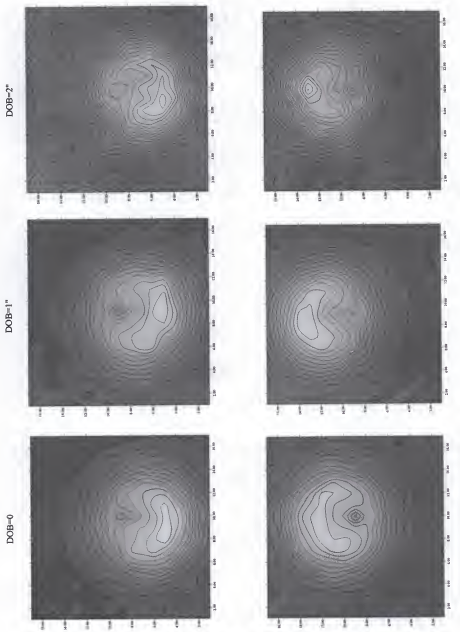

Figure 21. Forward and rear collimated detector images of a 12" plastic mine for DOB =0, 1", and 2".

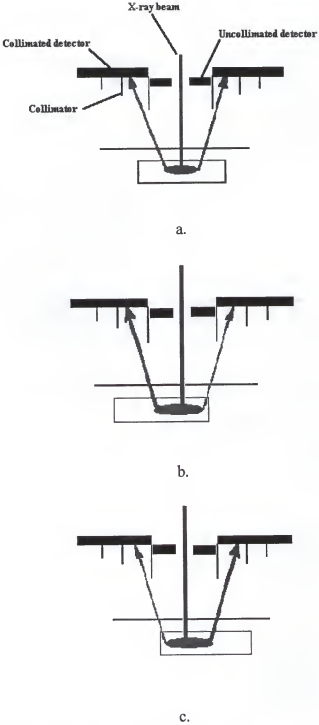

Figure 22. Visual representation of lateral migration to help discuss collimated detector image offsets.
a.) X-ray beam is at the center of the landmine. b.) X-ray beam is at the right side of the landmine. c.) X-ray beam is at the left side of the landmine.

The increase in offset ,due to lateral migration, as DOB increases is caused by the increase in the "source" of laterally migrated photons. This "source" is the first scattered photons that travel through the object. As the DOB increases the amount of scattering increases and causes the "source" to grow in size, though not in strength. The larger size of this source creates a larger offset to be apparent because the photon lateral migration path through the object is longer.

Detector Height Variations

The application of an LMR system to landmine detection presents many challenges. One of these is accounting for the possible variations in detector height including the change in solid angle effect and the change in collimator effectiveness caused by detector motion. Figures 23 and 24 show the case of a smooth surface with no buried features where the detector height was increased at a rate of 1/2" per foot of travel in the vehicle motion direction. The collimated detectors show a marked increase in detector response coinciding with the decreasing effectiveness of the collimators as the detector height was increased. The solid angle effect on the collimated detectors is masked by the increased number of first collision photons not being absorbed in the collimators. As expected, the uncollimated detectors show a pronounced decrease in detector response due to the r^2 dependence of the change in solid angle. The difference in response between the collimated and uncollimated detectors indicates the system should be able to detect landmines over rough terrain that could cause the detection vehicle to ride unevenly.

Measured Images

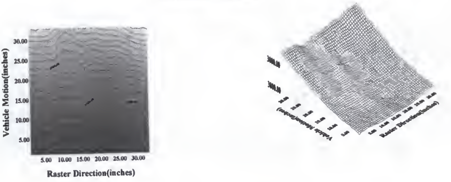

Front Detector Image

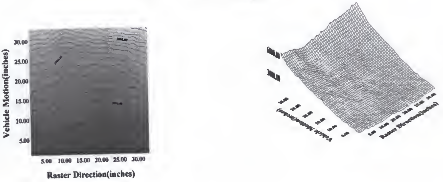

Rear Detector Image

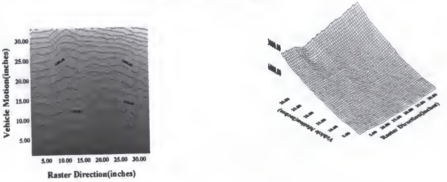

Sum of Two Detector Images

Figure 23. Collimated detector images, no landmine, detector height is raised 1/2" per foot of travel in the motion direction.

Measured Images

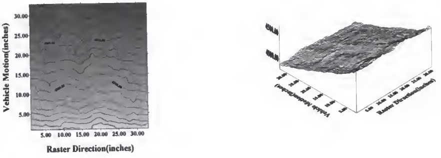

Front Detector Image

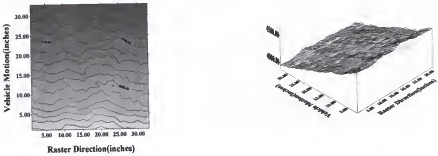

Rear Detector Image

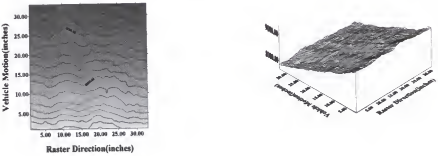

Sum of Two Detector Images

Figure 24. Uncollimated detector images, no landmine, detector height is raised 1/2" per foot of travel in the motion direction.

The characteristic that allows the LMR system to differentiate a change in detector height from an actual feature is that the collimated and uncollimated detectors respond inversely to a change in detector height. However, the collimated and uncollimated detectors respond in the same manner when material changes occur even in the presence of a height variation. Figure 25 shows a collimated detector image for the case of 1/2" increase in detector height per foot of forward motion with a 12" plastic mine at (16,16) DOB=1". Figure 26 shows the uncollimated detector image for the same experiment. In these images the landmine is still apparent even with the slope.

Using the characteristic that the collimated and uncollimated detectors respond in opposite manners, the effects caused by the slope can be removed. Figure 27 shows the results of applying the buried feature detection code to the original Figures 25 and 26. Table 9 gives the results calculated by the code.

Table 9. Slope Removeal Using the Buried Feature Detection Code

Parameters	Actual (in)	Calculated (in)	Difference (%)
X_o	16.00	16.16	1.00
Y_o	16.00	15.10	-5.63
X size	12.00	11.00	-8.33
Y size	12.00	13.00	8.33
Area	113.00	116.00	2.65

Measured Images

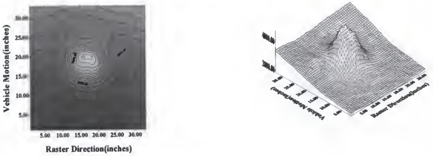

Front Detector Image

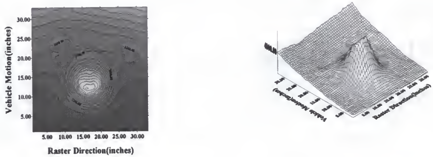

Rear Detector Image

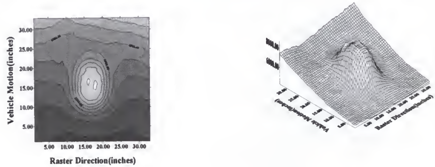

Sum of Two Detector Images

Figure 25. Collimated detector images, 12" plastic landmine at (16,16), detector height is raised 1/2" per foot of travel in the motion direction.

Measured Images

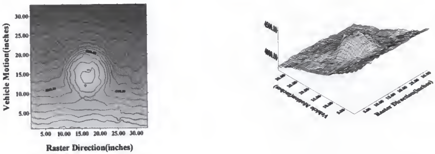

Front Detector Image

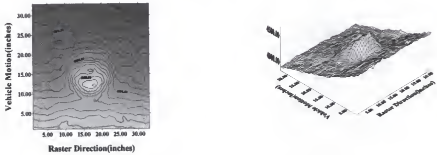

Rear Detector Image

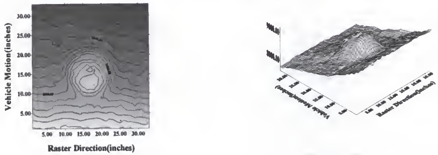

Sum of Two Detector Images

Figure 26. Uncollimated detector images, 12" plastic landmine at (16,16), detector height is raised 1/2" per foot of travel in the motion direction.

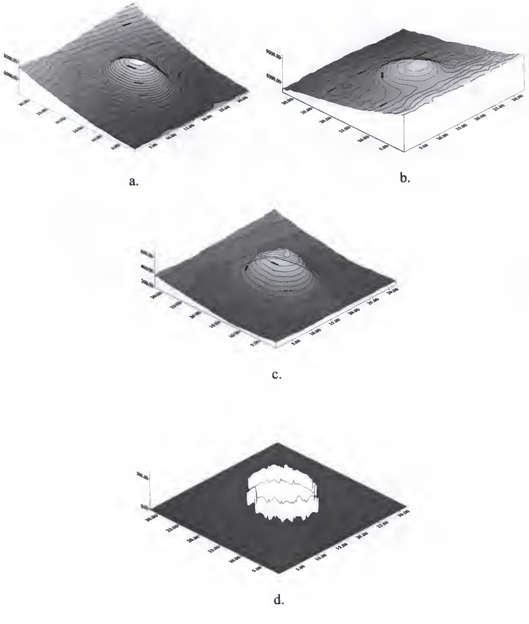

Figure 27. Inputs and outputs for the buried feature detection code implemented for the case of soil slope removal.
a.) Collimated detector input. b.) Uncollimated detector input. c.) Slope removed output. d.) Globbed image output

Surface Variations

When imaging unknown objects, surface variations create features in the images that could be incorrectly interpreted. The collimated detectors will respond to a depression in the surface in the same manner that they respond to an increase in detector height, with an increase in detector signal. The uncollimated detectors will respond to a depression in the surface with a decrease in detector response for the same reasons.

Surface variations that an LMR system applied to landmine detection are likely to encounter in the field are potholes, rocks, and dirt ridges. Ridges of dirt and rocks on the surface fall into the same category as most of the other surface features, i.e. sticks and man-made objects. These features can be removed from the image using the information from the collimated and uncollimated detectors as discussed earlier in the image processing section.

To test the LMR system a pothole that was ~1" deep and 12" across was created. Figure 28 shows the observed collimated detector images. Based on the information obtained from the collimated detector images it is not possible to determine if the object is a plastic mine or a pothole. Figure 29 shows the uncollimated detector images of the same pothole. The uncollimated detector images appear to contain the equivalent of a metal mine. The four-detector system allows the LMR system to differentiate between potholes and landmines using the information from both detectors sets. Potholes are identified due to the inverse response of the collimated and uncollimated detectors in the same way that variations in detector height are distinguished from image features.

Measured Images

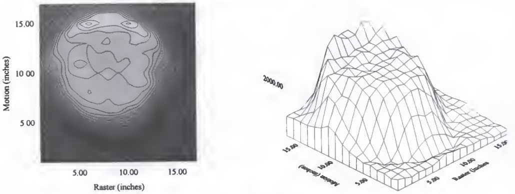

Front Detector Image

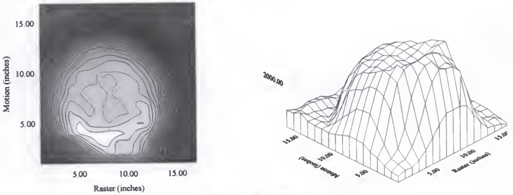

Rear Detector Image

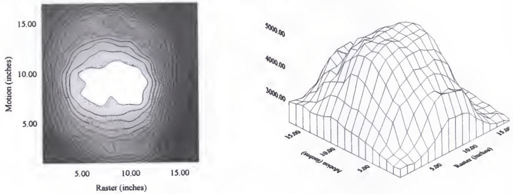

Sum of Two Detector Images

Figure 28. Collimated detector images of a 1" deep pothole.

Measured Images

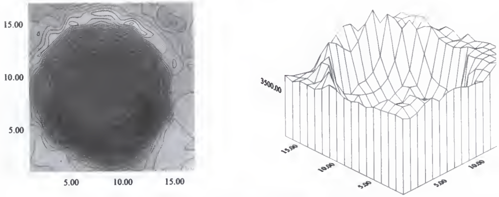

Front Detector Image

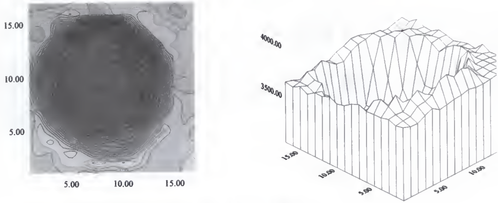

Rear Detector Image

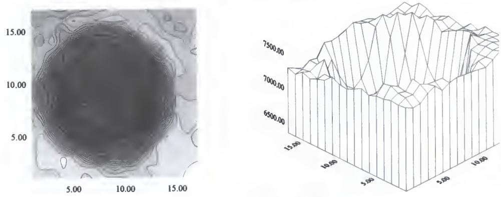

Sum of Two Detector Images

Figure 29. Uncollimated detector images of a 1" deep pothole.

Resolution Improvement

In an effort to improve the LMR system's ability to distinguish fine details (<1"), the pixel size was changed from 1" to 1/2" and then to 1/4". To evaluate the system's response, a 6" diameter 2.5" thick plastic disk with four holes (diameters of 2.5", 1.75", 1.25", and 0.75") was fabricated. Figure 30 shows the object in the same orientation as it appears in the subsequent images. For all images the holes were filled with sand. Figures 31 and 32 show the collimated and uncollimated detector responses, respectively, with 1/2" pixels, a x-ray spot size of 0.25 in^2 and a DOB=0". The three larger holes were apparent, but the 0.75" hole was too small to be reliably detected.

In order to detect the small hole, the pixel size was reduced to 1/4" and the x-ray spot size was reduced to 0.16 in^2. The optimal size x-ray beam size for 1/4" pixels would be 0.063 in^2, but the data acquisition system limited how small the spot size could be made. The number of photons emitted per second per pixel is directly related to pixel size, so in order to maintain the same statistical accuracy with a smaller pixel the power of the x-ray machine or the dwell time for each pixel must be increased. Since the Maxitron is an old x-ray machine a 10 mA current is the maximum permitted for a long run. At the necessary sampling rate the data acquisition system can only sample for 0.4 s before overflowing the storage buffer. This limited the size of the pixel to 0.16 in^2. Figures 33 and 34 show the collimated and uncollimated detector responses, respectively, with 1/4" pixels, a x-ray spot size of 0.16 in^2 and a DOB=0". The smaller hole can now be identified. Figure 35 shows the result of image segmentation upon the sum of the uncollimated detector images and all four holes are clearly visible.

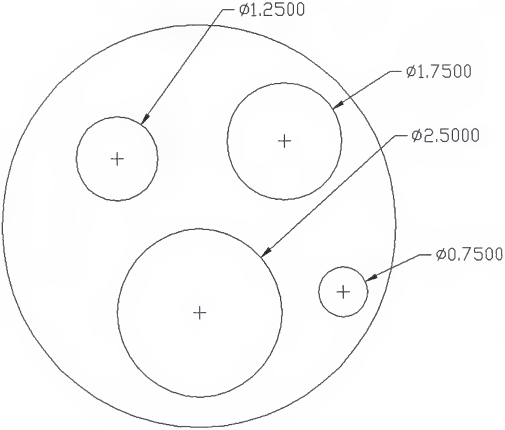

Figure 30. Plastic disk used for resolution improvement experiments.

Measured Images

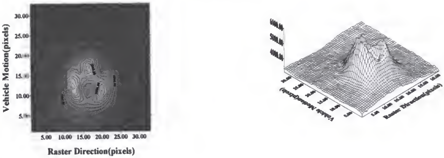

Front Detector Image

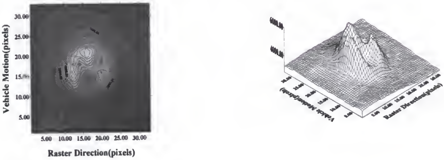

Rear Detector Image

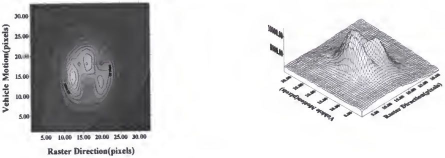

Sum of Two Detector Images

Figure 31. Collimated detector images of plastic disk using 1/2" pixels DOB=0.

Measured Images

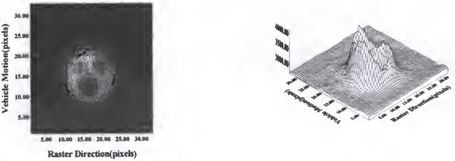

Front Detector Image

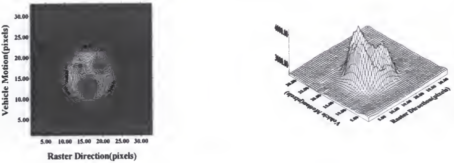

Rear Detector Image

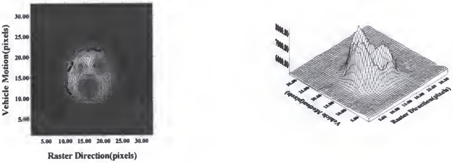

Sum of Two Detector Images

Figure 32. Uncollimated detector images of plastic disk using 1/2" pixels DOB=0.

Measured Images

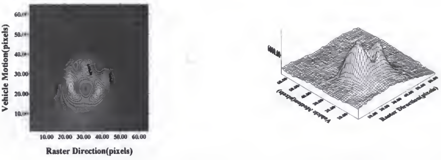

Front Detector Image

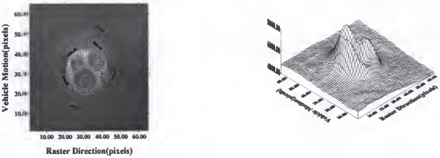

Rear Detector Image

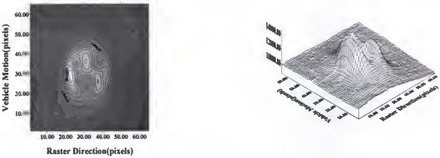

Sum of Two Detector Images

Figure 33. Collimated detector images of plastic disk using 1/4" pixels DOB=0.

Measured Images

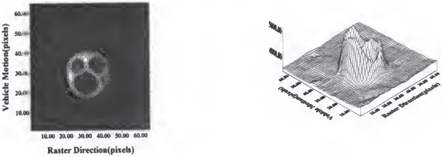

Front Detector Image

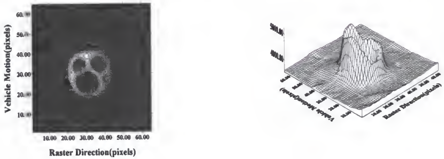

Rear Detector Image

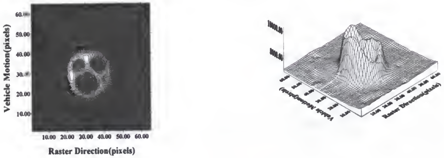

Sum of Two Detector Images

Figure 34. Uncollimated detector images of plastic disk using 1/4" pixels DOB=0.

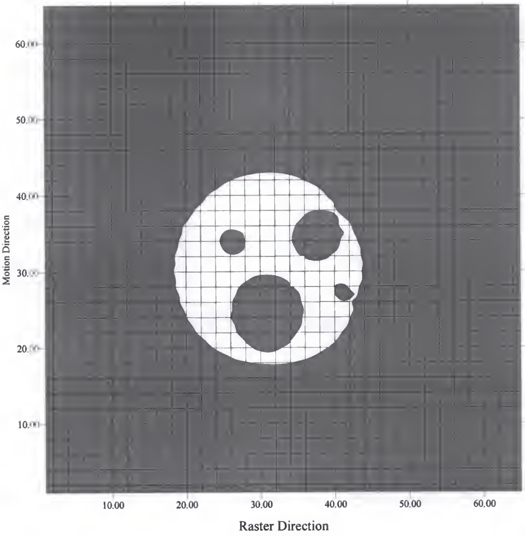

Figure 35. Segmented image of plastic disk with 1/4" pixels DOB=0.

The results from the 1/4" pixel DOB=0 images were better than expected. The resolution was somewhat limited because of the need to use an x-ray spot size that was too large. The large x-ray spot size will cause a lowpass filtering of the image to occur because the x-ray spot will illuminate features that are larger than the pixel size from both sides instead of just illuminating the pixel size. The segmented image seen in Figure 35 shows that the small features are still visible. This is possibly because segmentation may act as a sharpening filter. The selection of the threshold of segmentation can produce widely varied images. Figures 36 and 37 show the collimated and uncollimated detector responses, respectively, for the 1/4" pixel plastic disk setup with the DOB=1". Figure 38 shows the segmented image for the uncollimated detector response. The holes are all still visible, but the edges of the two holes on the right are no longer visible because less information from the disk reaches the detectors.

Pattern Recognition

The images that are produced by the LMR system contain information about the shape of the inspected objects. Using standard pattern recognition techniques it is possible to identify not only that there is an object, but whether the object matches a previous image. The surface and buried feature detection codes would be used first to locate the possible object and to identify the region of interest. The region of interest would be small enough to just contain one object to reduce the pattern recognition requirements. Since the region of interest would be centered around the object there is no

Measured Images

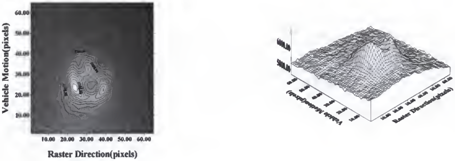

Front Detector Image

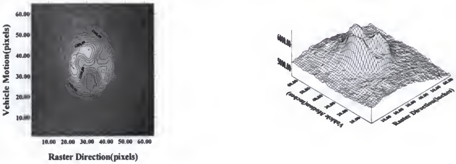

Rear Detector Image

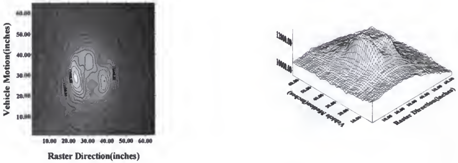

Sum of Two Detector Images

Figure 36. Collimated detector images of plastic disk using 1/4" pixels DOB=1".

Measured Images

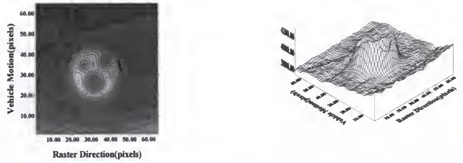

Front Detector Image

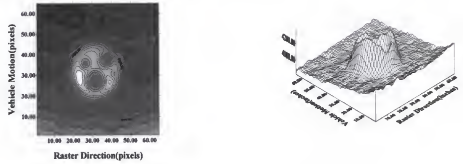

Rear Detector Image

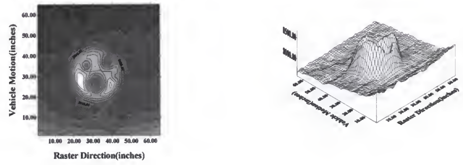

Sum of Two Detector Images

Figure 37. Uncollimated detector images of plastic disk using 1/4" pixels DOB=1".

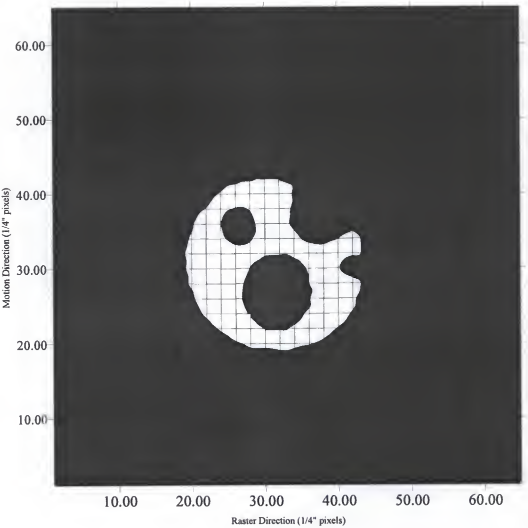

Figure 38. Segmented image of plastic disk with 1/4" pixels DOB=1".

need for the pattern recognition system to be translationally invariant; this again reduces the needed processing. The application of LMR to landmine detection precludes the need for scale invariance because it is important to be capable of distinguishing between different sizes of landmines. To test the viability of pattern recognition the uncollimated detector image shown in Figure 34 was used as the image to be compared for a possible match. Figure 39 shows the original target image (a) along with five test images: the original with a 90° rotation (b), the original with a 5 pixel shift in the x-direction (c), the original with a 5 pixel shift in the y-direction (d), a square image of the same outer dimensions as the original image (e), and a circular image with the same diameter of the original image (f). The square and the circular images were generated artificially and have the same maximum and minimum as the original image.

The pattern recognition code was implemented in MATLAB (see Appendix D). The 2-D Fourier transform of the original image was taken and then compared to the Fourier transform of the test images.[17] The Fourier transform was picked because it is a fast (low computational time) transform that converts a spatial image into a frequency image. The characteristic frequency is used to identify the images. The flow diagram for a possible pattern recognition code is given in Figure 40.

One problem with using the Fourier transform for pattern recognition is that the frequency transform rotates the same amount as the spatial image. If the image is rotated 90° then the Fourier transform of the image is also rotated 90°. This will be addressed in the method used to calculate the difference in the images. The standard method of

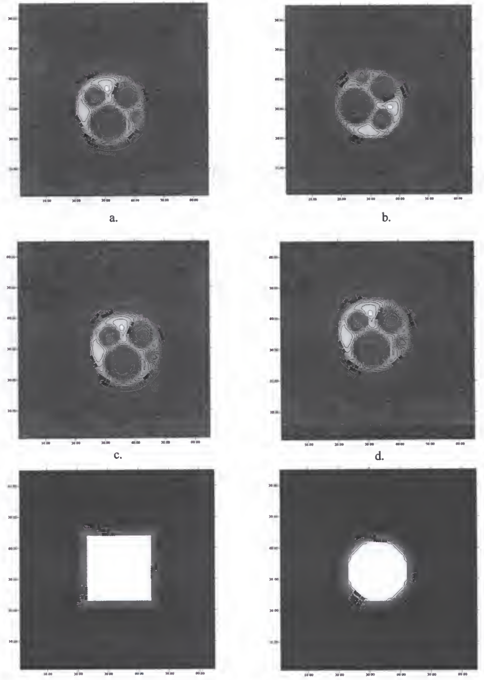

a.

b.

c.

d.

e.

f.

Figure 39. Images used in the evaluation of the pattern recognition system.
a.) Original image b.) Rotated image c.) X-translated image d.) Y-translated image
e.) Square image f.) Circular image.

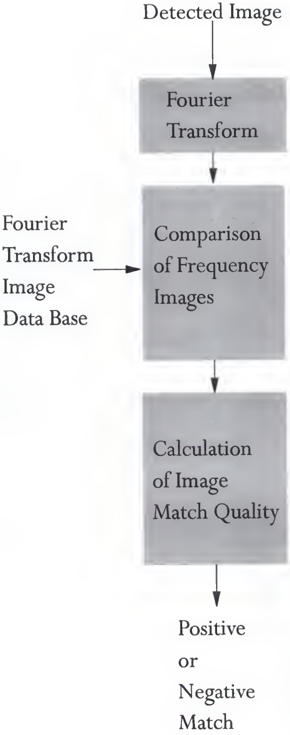
Detected Image
Fourier Transform
Fourier Transform Image Data Base
Comparison of Frequency Images
Calculation of Image Match Quality
Positive or Negative Match

Figure 40. Flow diagram of possible pattern recognition code.

Table 10. The sum of the absolute value of the magnitude differences.

Case	Rotated	X-Translated	Y-Translated	Square	Circle
Difference	1.35e+6	8.80e+4	1.77e+5	2.09e+7	1.95e+7
Match Quality	93	99	99	0	7

finding the difference between two images is to sum the absolute value of the magnitude differences. The results of this method are given in Table 10. Although the difference between the rotated image and the original image is large it is still an order of magnitude less then the square or the circular image differences. Another method of finding the difference is to just take the sum of the differences. Table 11 shows the results of this approach. The rotated difference is so small because of the equal rotation of the Fourier transform and the spatial image. For every point in the image with a negative difference there is a point with an equal positive difference. The small value that does occur is caused by computer round-off error. The differences between the translated images and the square and the circular image are still at least an order of magnitude so that an object could be identified with a high degree of confidence. For determination of a match, a difference of less then $3x10^6$ or a match quality of over 80 would constitute a match for both methods. The criteria that determined the maximum difference was set by

Table 11. The the sum of the magnitude differences.

Case	Rotated	X-Translated	Y-Translated	Square	Circle
Difference	4.15e-9	6.34e+4	2.13e+6	2.13e+7	1.85e+7
Match Quality	100	99	90	0	13

comparing the differences for the three images that should match to the differences of the two images that should not.

Figure 41 shows the centered logarithmic zero-crossings of the magnitude of the Fourier transforms for the original and test images. The rotational characteristic of theFourier transform is clearly evident in Figure 41b. The difference between the frequency contours for the shifted images is not obvious to the human eye (Figures 41c. and 41d.) even though a large difference is apparent when mathematically comparing images. The differences in the contours for the circle and the square images (Figures 41e and 41f) are very clear and explains the high values for the differences.

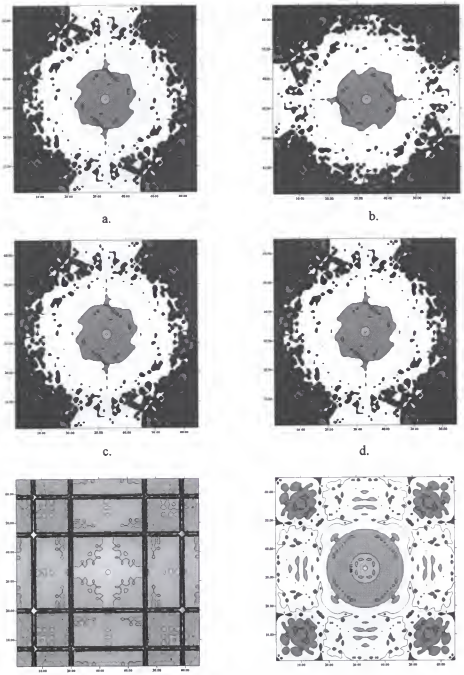

a. b. c. d. e. f.

Figure 41. Frequency zero-crossings for the images used in the evaluation of the pattern recognition system.
a.) Original image b.) Rotated image c.) X-translated image d.) Y-translated image e.) Square image f.) Circular image.

CHAPTER 5
CONCLUSIONS

CBI systems that use only collimated detectors are capable of imaging objects and creating images that contain information about the surface and the subsurface objects. Conventional CBI systems do, however, have low information-carrying photon detection efficiency and can not separate the surface and subsurface objects from generated images. The addition of uncollimated detectors to the collimated detectors of the CBI system created the LMR system, which allows knowledge to be gathered by the system to differentiate between surface and subsurface objects by algebraic combination of the detector responses. This was made possible because the uncollimated detectors' response is dominated by photons carrying information about the surface features and the collimated detectors' response includes information about both the subsurface and surface features.

The change to a large area detector array using varying degrees of collimation solves not only the surface feature clutter problem, but it also permits LMR systems to account for changes in detector height variation, surface heterogeneties, and increase detector efficiency. The LMR system's ability to remove the effects of detector height variation propagates from the differences in responses for the collimated and uncollimated detectors. The uncollimated detector's response to changes in detector height are directly related to the change in solid angle that the detector sees. If the uncollimated detector height increases the detector response will decrease, and vica versa.

The collimated detector response is more complicated. The collimated detector is also affected by the change in solid angle of the system, but the change in collimator effectiveness dominates the detector response. When the collimated detector height increases the collimators become less effective and the collimated detector starts to respond to photons that have had only one interaction. Since this is a large signal compared to the signal from photons with multiple collisions (one order of magnitude larger) the collimated detector signal will increase as the detector height increases. If the collimated detector height decreases the detector becomes over collimated because the collimators will start to filter out photons that have laterally migrated through the objects and the detector response will decrease.

The large area of the detectors, 144 in^2 for the collimated and 48 in^2 for the uncollimated, increases the efficiency of the LMR systems utilization of information carrying photons. The large area of the detectors also minimizes the effects of small heterogeneities, removing another noise component from the images.

The resolution of the images generated with the LMR system can be varied to either optimize image generation speed, necessary x-ray machine power, or image resolution. The maximum resolution of an LMR system is limited by the medium in which it will be used and must be evaluated for different situations. Some of the influencing factors would be the atomic number (Z) of the medium, the difference between the Z of the expected objects and the Z of the medium, and the maximum depth that the LMR system would be expected to function.

In order to evaluate the LMR system it was applied to the problem of landmine detection. Landmine detection provides a good test for the LMR system because it requires the use of a backscatter modality, the possibility of unknown surface clutter, varying target material, the ability to identify regions of interest, and the need for a system that creates images.

The LMR landmine detection system was shown to be capable of detecting both metal and plastic landmines at depths of up to 3 inches. Using the relationship between the collimated and uncollimated detectors, features on the surface could be located and identified. After the surface features were removed, the buried features could be identified. Because the LMR system produces images of the scanned objects it is possible to use pattern recognition algorithms to allow the system to not only locate the possible landmines, but identify the landmine if an image of the detected landmine is stored in the system's database.

Detectors used in the LMR system were evaluated to improve the system functional capabilities while decreasing its weight and increasing its robustness. Advances in PM-tube technologies provided improved light sensing elements that allowed the new detector design to retain the high gain and low dark current of a PM-tube while only having a small vacuum tube. This improved the detectors' overall resistance to damage from shock or impact. Flat scintillator screens allowed the new detector design to remain light weight, but the efficiency was much lower than the standard plastic scintillators. Typical 2" thick plastic scintillator are ~90% efficient (optical photons out/x-ray photons in) while the thin screens are ~1.5%. Improvements such as attaching the screen scintillators to the sides of the detectors instead of just the bottom could provide a two to four-fold increase in total detector efficiency. Using multiple fins could also increase the apparent efficiency of the detector by an order of magnitude or more.

To decrease the amount of time required to collect data for each pixel, the largest pixel size possible for a given resolution should be used. For landmine detection, using 1" pixels is sufficient for the detection of landmines 6" diameter or larger, though small details (less than 3 pixels) on landmines will be lost. The system will respond to smaller objects, but little information about size and shape will be collected. Using 1/4" pixels the LMR system is capable of detecting a 0.75" diameter object even while using a 0.16 in^2 spot size. The ability to use different resolutions is an advantage, but it also requires some knowledge of the objects to be encountered. If the possible objects in the area are unknown, the smallest resolution would need to be used.

The LMR system as applied to landmine detection was able to function in areas that had varied terrain slopes or potholes because the information provided by the collimated and uncollimated detectors allowed the changes in detector height to be differentiated from surface or buried objects. Working in different geographical regions could pose a problem when dealing with various soil types. In areas that contain high concentrations of iron or other heavy metals, the LMR system's maximum detectable DOB will be less than the standard 3" that is possible in sandy soil. Increasing the x-ray energy above 175 keV may be useful for soil variations that restrict the maximum DOB, but it would lower the efficiency of the system and increase the demand on the x-ray generator.

The LMR system when applied to landmine detection registers absorbing objects large enough to cover a possible landmine as false positives. This is because a lack of backscatterd photons furnishes no information about objects below the absorber. A possible remedy would be to combine the LMR landmine detection system with another detection system. A chemical sniffer could be used to check for chemical residue indicating explosives and help to eliminate false positives. Utilizing the LMR as the locator of points of interest would allow the system to proceed at a reasonable speed without continuously operating the chemical sniffer. False positives could also be reduced by the creation of a landmine detector database containing images of possible landmines that the system could compare to and use to identify detected objects.

The application of the LMR system to landmine detection has shown that the LMR system has many potential features that could be useful in other areas such as non-destructive inspection or examination applications. The LMR system will be useful for applications that are looking for features or trends in objects that are on the order of the mean-free-path of the photon in the object. An example might be that a part has fibers imbedded in it, if the fibers run in a specific direction an LMR system could determine that even if it could not resolve the individual fibers. The LMR system will not be effective in applications where the features are significantly smaller then the mean-free-path of the photon in the object. Additional investigations into the maximum achievable resolution of the LMR system in different media could establish where the system would be useful in quality control.

APPENDIX A

MOTION CONTROL AND DATA ACQUISITION SYSTEM CODE

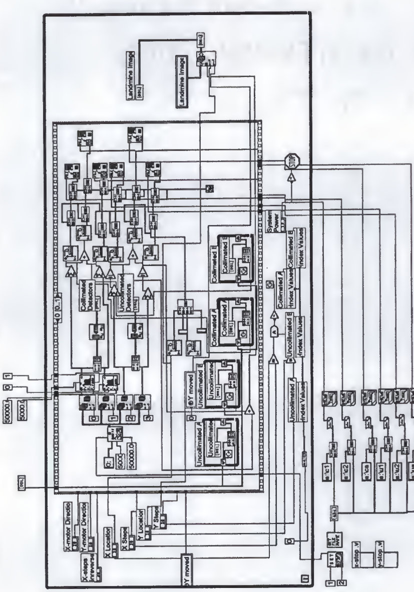

Figure A-1. LabView code for data acquisition and motion control system.

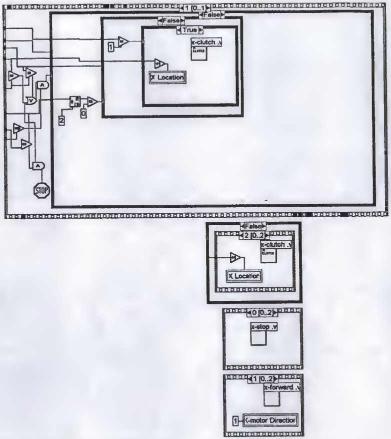

Figure A-2. LabView code for data acquisition and motion control system .

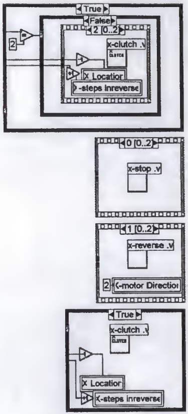

Figure A-3. LabView code for data acquisition and motion control system .

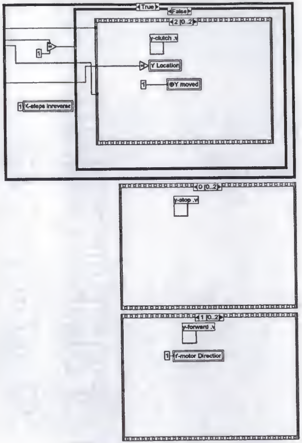

Figure A-4. LabView code for data acquisition and motion control system .

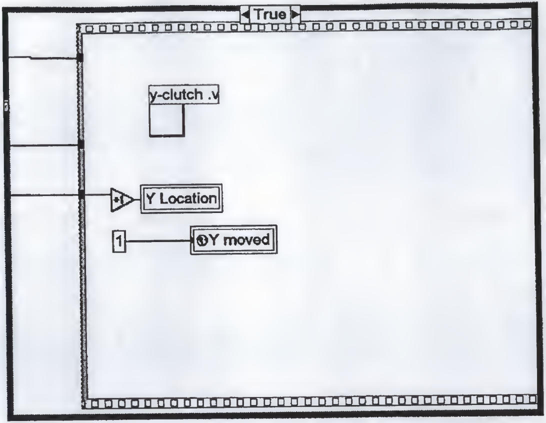

Figure A-5. LabView code for data acquisition and motion control system .

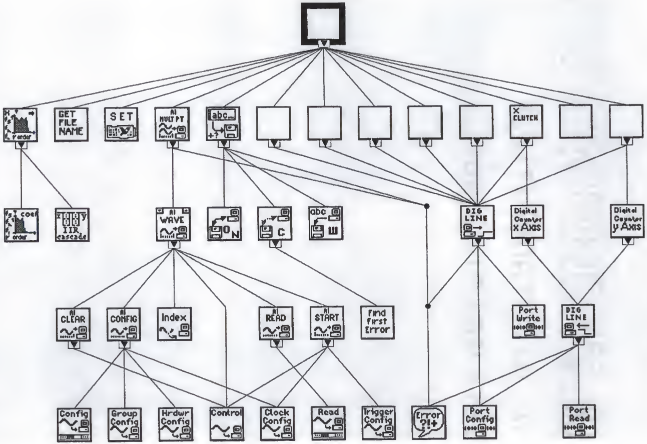

Figure A-6. LabView code for data acquisition and motion control system .

APPENDIX B
SURFACE FEATURE DETECTION CODE

```
PRO surfrem,xd,yd,path,file
RED=[0,1,1,0,0,1]
GREEN=[0,1,0,1,0,1]
BLUE=[0,1,0,0,1,0]
TVLCT,255*RED,255*GREEN,255*BLUE



on_error,1
nparams=n_params()
if nparams eq 0 then begin
        print,'Format: surfrem,xd,yd,"path","filename"'
        print,'xd is the x dimenion for the input files'
        print,'yd is the y dimenion for the input files'
        print,'Path must end with \ eg. c:\data\'
        print,'Filename in this case is the data mark without the c1...'
        return
endif
z1=replicate(0,xd,yd)
z2=replicate(0,xd,yd)
z3=replicate(0,xd,yd)
z4=replicate(0,xd,yd)
file=string(file)
path=string(path)
fcoll=strcompress(path+'c2'+file,/remove_all)
rcoll=strcompress(path+'c1'+file,/remove_all)
funcoll=strcompress(path+'u2'+file,/remove_all)
runcoll=strcompress(path+'u1'+file,/remove_all)
i=0
; Reading in the data files
openr,unit1,fcoll, /get_lun
while (not eof(unit1)) do begin
        readf,unit1,x,y,zr
        z1(x-1,y-1) = zr
endwhile
```

```
openr,unit2,rcoll, /get_lun
while (not eof(unit2)) do begin
        readf,unit2,x,y,zr
        z2(x-1,y-1) = zr
endwhile
openr,unit3,funcoll, /get_lun
while (not eof(unit3)) do begin
        readf,unit3,x,y,zr
        z3(x-1,y-1) = zr
endwhile
openr,unit4,runcoll, /get_lun
while (not eof(unit4)) do begin
        readf,unit4,x,y,zr
        z4(x-1,y-1) = zr
endwhile

;Start of the lowpass filter section
filter=replicate(1,3,3)
fz1=convol(z1,filter,9)
fz2=convol(z2,filter,9)
fz3=convol(z3,filter,9)
fz4=convol(z4,filter,9)
fz1=fz1(1:31,1:31)
fz2=fz2(1:31,1:31)
fz3=fz3(1:31,1:31)
fz4=fz4(1:31,1:31)
;end of the lowpass filter section

;Start of Surface feature detection section
z3max=max(fz3)
z4max=max(fz4)
z3min=min(fz3)
z4min=min(fz4)
dz3=z3max-z3min
dz4=z4max-z4min
az3=total(fz3)/((yd-1)*(xd-1))
az4=total(fz4)/((yd-1)*(xd-1))
hcz3=1.1*az3
lcz3=.995*az3
hcz4=1.1*az4
lcz4=.995*az4

spglob=replicate(0,xd,yd)
smglob=replicate(0,xd,yd)
spold=replicate(0,xd,yd)
```

```
smold=replicate(0,xd,yd)
count=0
for i=1,xd-3 do begin
        for j=1,yd-3 do begin
                count=count+1
                if (fz3(i,j) ge hcz3) then spglob(i,j)=count
                if (fz3(i,j) le lcz3) then smglob(i,j)=count
                if (fz4(i,j) ge hcz4) then spglob(i,j)=count
                if (fz4(i,j) le lcz4) then smglob(i,j)=count
        endfor
endfor
done='N'
Jump1: while (done ne 'Y') do begin
        for i=1,xd-2 do begin
                for j=1,yd-2 do begin
                        spold(i,j)=spglob(i,j)
                        smold(i,j)=smglob(i,j)
                        if (spglob(i,j) gt 0) then spglob(i,j)=spglob(i,j)>$
                        spglob(i+1,j)>spglob(i-1,j)>spglob(i,j+1)>spglob(i,j-1)
                        if (smglob(i,j) gt 0) then smglob(i,j)=smglob(i,j)>$
                        smglob(i+1,j)>smglob(i-1,j)>smglob(i,j+1)>smglob(i,j-1)
      endfor
   endfor
   for i=1,xd-2 do begin
        for j=1,yd-2 do begin
        if(spold(i,j) ne spglob(i,j)) then begin
                done='N'
                GOTO, Jump1
        endif
        if (smold(i,j) ne smglob(i,j)) then begin
                done='N'
                GOTO, Jump1
        endif else begin
                        done='Y'
      endelse
      endfor
   endfor
endwhile

;Start of Minimum size for Glob section
minsize=1
spe=replicate(0,xd*yd)
spmaxn=replicate(0,xd*yd)
spxinf=replicate(0,xd*yd,xd*yd)
spyinf=replicate(0,xd*yd,xd*yd)
```

```
sme=replicate(0,xd*yd)
smmaxn=replicate(0,xd*yd)
smxinf=replicate(0,xd*yd,xd*yd)
smyinf=replicate(0,xd*yd,xd*yd)
for i=1,xd-2 do begin
    for j=1,yd-2 do begin
        for l=1,xd*yd-1 do begin
            if (spglob(i,j) eq l) then spe(l)=spe(l)+1
            if (smglob(i,j) eq l) then sme(l)=spe(l)+1
   endfor
    endfor
endfor

for l=1,xd*yd-1 do begin
    if (spe(l) lt minsize) then begin
        spe(l)=0
        for i=1,xd-2 do begin
            for j=1,yd-2 do begin
                if (spglob(i,j) eq l) then spglob(i,j)=0
            endfor
        endfor
    endif else begin
        n=0
        for i=1,xd-2 do begin
            for j=1,yd-2 do begin
                if (spglob(i,j) eq l) then begin
                    n=n+1
                    spmaxn(l)=spmaxn(l)>n
                    spxinf(l,n)=i
                    spyinf(l,n)=j
                endif
            endfor
        endfor
    endelse
if (sme(l) lt minsize) then begin
        sme(l)=0
        for i=1,xd-2 do begin
            for j=1,yd-2 do begin
                if (smglob(i,j) eq l) then smglob(i,j)=0
            endfor
        endfor
    endif else begin
        n=0
        for i=1,xd-2 do begin
            for j=1,yd-2 do begin
```

```
                        if (smglob(i,j) eq l) then begin
                            n=n+1
                            smmaxn(l)=smmaxn(l)>n
                            smxinf(l,n)=i
                            smyinf(l,n)=j
                        endif
                    endfor
                endfor
            endelse
endfor

;Start of the section that compiles the information about
;the landmines
spgnum=0
smgnum=0
for l=1,xd*yd-1 do begin
    spxtotal=0
    smxtotal=0
    spytotal=0
    smytotal=0
    spmaxx=0
    smmaxx=0
    spmaxy=0
    smmaxy=0
    spminx=xd-1
    smminx=xd-1
    spminy=yd-1
    smminy=yd-1
    if (spe(l) ne 0) then begin
        spgnum=spgnum+1
        for n=1,spmaxn(l) do begin
            spmaxx=spxinf(l,n)>spmaxx
            spmaxy=spyinf(l,n)>spmaxy
            spminx=spxinf(l,n)<spminx
            spminy=spyinf(l,n)<spminy
            spxtotal=spxtotal+spxinf(l,n)
            spytotal=spytotal+spyinf(l,n)
        endfor
    endif
  if (sme(l) ne 0) then begin
        smgnum=smgnum+1
        for n=1,smmaxn(l) do begin
            smmaxx=smxinf(l,n)>smmaxx
            smmaxy=smyinf(l,n)>smmaxy
            smminx=smxinf(l,n)<smminx
```

```
                    smminy=smyinf(l,n)<smminy
                    smxtotal=smxtotal+smxinf(l,n)
                    smytotal=smytotal+smyinf(l,n)
               endfor
          endif
          if (spe(l) ne 0) then begin
               spx0=spxtotal/spe(l)
               spy0=spytotal/spe(l)
               spxaxis=spmaxx-spminx+1
               spyaxis=spmaxy-spminy+1
               sparea=spe(l)
               Print,'Surface Plastic Mine Information'
               print,'Glob Number           =',spgnum
               print,'Glob Area             =',sparea
               print,'Xo                    =',spx0
               print,'Yo                    =',spy0
               print,spmaxx,spminx,spmaxy,spminy
          endif
          if (sme(l) ne 0) then begin
               smx0=smxtotal/spe(l)
               smy0=smytotal/spe(l)
               smxaxis=smmaxx-smminx+1
               smyaxis=smmaxy-smminy+1
               smarea=sme(l)
               Print,'Surface Metal Mine Information'
               print,'Glob Number           =',smgnum
               print,'Glob Area             =',smarea
               print,'Xo                    =',smx0
               print,'Yo                    =',smy0
               print,smmaxx,smminx,smmaxy,smminy
          endif
endfor

!p.multi=[0,2,3,0,0]
print,az3,az4
print,lcz3,lcz4
print,hcz3,hcz4
print,min(smglob),max(smglob)
print,min(fz3),max(fz3)
surface,fz3,background=1,color=0
surface,z3,background=1,color=0
;set_plot,'ps'
;device,/encapsulated,filename='c:\joe\image1.ps'
surface,fz1,background=1,color=0
surface,z1,background=1,color=0
```

```
surface,spglob,background=1,color=0
surface,smglob,background=1,color=0
;device,/close
free_lun,unit1,unit2,unit3,unit4
end
```

APPENDIX C
BURIED FEATURE DETECTION CODE

```
!ccccccccccccccccccccccccccccccccccccccccccccccccccccccccccccccccc
!              SURREM41.F90                    c
!ccccccccccccccccccccccccccccccccccccccccccccccccccccccccccccccccc
!----------------------------------------------------------------
!     This code takes the Added Collimated and the Added
!     Uncollimated detector images and uses the information
!     to remove the surfaces features
!
!     This code is currently set to read 33X33
!     to change this set it and jt to new matrix size !
!----------------------------------------------------------------
!     Matrix Sizes
parameter(it=33,jt=33)
parameter(ntt=(it-1)*(jt-1))
!     Image Processing constants
!     sfc is the scaling factor for the collimated detectors
!     sfu is the scaling factor for the collimated detectors
!     cutoff is the scaling factor for the collimated detectors
parameter(sfc=1,sfu=1)
character*2 filtertype,repeat
character*40 colf,uncolf,output,globout
integer col(it,jt),uncol(it,jt),x,y,z,out(it,jt),rdstat,done
integer ncol(it,jt),nucol(it,jt),glob(it,jt),old(it,jt),e(ntt)
integer xinf(ntt,ntt),yinf(ntt,ntt),fcol(it,jt),funcol(it,jt)
integer umax,umin,udiff,cmax,cmin,cdiff,hfcol(it,jt)
integer hfuncol(it,jt),hcutoff,lcutoff,maxn(ntt)
real area,norm
!----------------------------------------------------------------
!     Reading in the File names and the data
!----------------------------------------------------------------
write(*,'(//,a)')                              &
&  ' ** Enter Collimated detector file name **'
print *,' '
read(*,*) colf
open(unit=1,status='old',file=colf)
write(*,'(//,a)')                              &
```

```
& ' ** Enter Uncollimated detector file name **'
print *,' '
read(*,*) uncolf
open(unit=2,status='old',file=uncolf)
write(*,'(//,a)')                          &
& ' ** Enter output file name **'
print *,' '
read(*,*) output
        write(*,'(//,a)')                          &
& ' ** Enter glob output file name **'
print *,' '
read(*,*) globout

rdstat=0
do while (rdstat .ne. -1)
        read(unit=1,fmt=*,iostat=rdstat) x,y,z
        col(x,y)=z
end do
rdstat=0
do while (rdstat .ne. -1)
        read(unit=2,fmt=*,iostat=rdstat) x,y,z
        uncol(x,y)=z
end do
!     While loop that repeats processing algorithm until operator
!     is satisfied
repeat="y"
do while (repeat .eq."y" .or. repeat .eq. "Y")
tout=0
open(unit=3,status='replace',file=output)
open(unit=4,status='replace',file=globout)
!----------------------------------------------------------------------
!     Starting Filter Options
!----------------------------------------------------------------------
 200    print *,' ** Pick Filter Option **'
print *,' ** L  =    Lowpass filter'
print *,' ** HB =    Highboost filter'
print *,' ** N  =    No Filtering'
print *,' '
print *,' ** Enter Option  '
read(*,*) filtertype
!     Start of Lowpass filter
if (filtertype .eq. "L" .or. filtertype .eq."l") then
        print *,'Lowpass filtering done to images'
        do i=1,it-1
                do j=1,jt-1
```

```
                    fcol(i,j)=(col(i,j)+col(i+1,j)        &
&                +col(i,j+1)+col(i+1,j+1))/4
                    funcol(i,j)=(uncol(i,j)+uncol(i+1,j)   &
&                +uncol(i,j+1)+uncol(i+1,j+1))/4
            end do
        end do
!     Start of Highboost filter
elseif (filtertype .eq. "HB" .or. filtertype .eq."hb") then
        print *,'Highboost filtering done to images'
        do i=1,it-1
            do j=1,jt-1
                    hfcol(i,j)=(col(i,j)+col(i+1,j)        &
&                +col(i,j+1)+col(i+1,j+1))/4
                    hfuncol(i,j)=(uncol(i,j)+uncol(i+1,j)   &
&                +uncol(i,j+1)+uncol(i+1,j+1))/4
                    fcol(i,j)=col(i,j)-hfcol(i,j)
                    funcol(i,j)=uncol(i,j)-hfuncol(i,j)
            end do
        end do
elseif (filtertype .eq. "N" .or. filtertype .eq."n") then
        print *,'No filtering done to images'
        do i=1,it-1
            do j=1,jt-1
                    fcol(i,j)=col(i,j)
                    funcol(i,j)=uncol(i,j)
            end do
        end do



        goto 299
        else
        print *,'You have not selected a possible option'
        goto 200 299     endif
!-------------------------------------------------------------------
!     Ending Filter Options
!-------------------------------------------------------------------
!-------------------------------------------------------------------
!     Starting the subtraction Algorithm
!-------------------------------------------------------------------
cmax=0
umax=0
do i=1,it-1
        do j=1,jt-1
                if (fcol(i,j) .ge. cmax) cmax=fcol(i,j)
                if (funcol(i,j) .ge. umax) umax=funcol(i,j)
        end do
end do
!     Debuging info
!      print *,'The max collimated pixel value for the processed image is'
!      print 1001, cmax !1001    format (i5)
!      print *,'The max uncollimated pixel value for the processed image is'
!      print 1001, umax
cmin=cmax
umin=umax
do i=1,it-1
        do j=1,jt-1
                if (fcol(i,j) .lt. cmin) cmin=fcol(i,j)
                if (funcol(i,j) .lt. umin) umin=funcol(i,j)
        end do
end do
cdiff=cmax-cmin
udiff=umax-umin
norm=cdiff/udiff
omin=0
do i=1,it-1
        do j=1,jt-1
                ncol(i,j)=norm*sfc*255*(fcol(i,j)-cmin)/cdiff
                nucol(i,j)=sfu*255*(funcol(i,j)-umin)/udiff
                out(i,j)=ncol(i,j)-nucol(i,j)
                if (out(i,j) .le. omin) omin=out(i,j)
        end do
end do
        do i=1,it-2
                do j=1,jt-2
                        out(i,j)=(out(i,j)+out(i+1,j)        &
&                  +out(i,j+1)+out(i+1,j+1))/4
                end do
        end do



do i=1,it-1
        do j=1,jt-1
                out(i,j)=out(i,j)+abs(omin)
                write(unit=3,fmt=*) i,j,out(i,j)
                tout=tout+out(i,j)
        end do
end do
avgout=tout/ntt
```

```
print *,'The average pixel value for the processed image is'
print 1000, avgout 1000    format (f12.5)
print *,'Enter the desired high cutoff value: '
read(*,*) hcutoff
print *,'Enter the desired low cutoff value: '
read(*,*) lcutoff
!---------------------------------------------------------------------
!      End of the surface feature subtraction Algorithm
!      Start of the Globing Algorithm
!---------------------------------------------------------------------
!      Variables used in algorithm
count=0
done=0
!      Setup glob matrix to zeros

do i=1,it-1
        do j=1,jt-1
                glob(i,j)=0
        end do
end do
!      Finding pixels of interest
        do i=1,it-1
        do j=1,jt-1
                count=count+1
                if (out(i,j) .ge. hcutoff) then
                        glob(i,j)=count
                end if
                if (out(i,j) .le. lcutoff) then
                        glob(i,j)=count
                end if
                end do
end do
!      Globing pixels together in 4-contectility
100    if (done .ne. 1) then

do i=1,it-1
        do j=1,jt-1
                old(i,j)=glob(i,j)
                if (glob(i,j) .gt. 0) then
                        glob(i,j)=max(glob(i+1,j),glob(i-1,j),  &
&                           glob(i,j+1),glob(i,j-1),glob(i,j))
                end if
        end do
end do
do i=1,it-1
```

```
        do j=1,jt-1
                if (old(i,j) .ne. glob(i,j)) then
                        done=0
                        goto 100
                else
                        done=1
                end if
        end do
end do
goto 100
else
end if
!---------------------------------------------------------------------
!       End of Globing Algorithm
!---------------------------------------------------------------------
!---------------------------------------------------------------------
!       Start of Minimum Size for Glob
!---------------------------------------------------------------------
!       minsize=minimum number of coneccted pixels it
!       takes to be a real glob
minsize=3
!       set e(l) to all zeros
do l=1,ntt
        e(l)=0
end do
!       ntt=total max counts

do i=1,it-1
        do j=1,jt-1
                do l=1,ntt
                        if (glob(i,j) .eq. l) then
                                e(l)=e(l)+1
                        end if
                end do
        end do
end do
        do l=1,ntt
        if (e(l) .lt. minsize) then
                e(l)=0
                do i=1,it-1
                        do j=1,jt-1
                            if (glob(i,j) .eq. l) glob(i,j)=0
                        end do
                end do
        else
```

```
!----------------------------------------------------------------------
!     Start of the loop that gets the x and y info
!----------------------------------------------------------------------
                n=0
                maxn(l)=0
                do i=1,it-1
                        do j=1,jt-1
                                if (glob(i,j) .eq. l) then
                                        n=n+1
                                        if (n .gt. maxn(l))     &     &
 maxn(l)=n
                                        xinf(l,n)=i
                                        yinf(l,n)=j
                                end if
                        end do
                end do
!----------------------------------------------------------------------
!     End of the loop that gets the x and y info
!----------------------------------------------------------------------
        end if
end do
!----------------------------------------------------------------------
!     End of Minimum Size for Glob
!----------------------------------------------------------------------
!----------------------------------------------------------------------
!     Start of code that prints out information
!----------------------------------------------------------------------
        gnum=0
do l=1,ntt
        xtotal=0
        ytotal=0
        maxx=0
        maxy=0
        minx=it-1
        miny=jt-1
        if (e(l) .ne. 0) then
                gnum=gnum+1
                do n=1,maxn(l)
                        if(xinf(l,n) .gt. maxx) maxx=xinf(l,n)
                        if(yinf(l,n) .gt. maxy) maxy=yinf(l,n)
                        if(xinf(l,n) .le. minx) minx=xinf(l,n)
                        if(yinf(l,n) .le. miny) miny=yinf(l,n)
                        xtotal=xtotal+xinf(l,n)
                        ytotal=ytotal+yinf(l,n)
                end do
        end if
        if (e(l) .ne. 0) then
                x0=xtotal/e(l)
                y0=ytotal/e(l)
                xaxis=maxx-minx+1
                yaxis=maxy-miny+1

        area=e(l)
        print *, "Glob Number           = ",gnum
        print *, "Glob Area             = ",area
        print *, "Xo                    = ",x0
        print *, "Yo                    = ",y0
        print *, "X axis size           = ",xaxis
        print *, "Y axis size           = ",yaxis
        print *,maxx,minx,maxy,miny
        print *
        end if
end do
!-------------------------------------------------------------------
!     End of code that prints out information
!-------------------------------------------------------------------

do i=1,it-1
        do j=1,jt-1
                write(unit=4,fmt=*) i,j,glob(i,j)
        end do
end do
close(3)
close(4)
print *,'Enter Y to repeat calculation anything else to quit: '
read (*,*) repeat
end do
end
```

APPENDIX D
PATTERN RECOGNITION CODE

```
%Pattern recognition code
%Sets the file ids for the ouput
fidf = fopen('fake.dat','w');
fidd = fopen('disk.dat','w');
fidr = fopen('rotate.dat','w');
fidx = fopen('tranx.dat','w');
fidy = fopen('trany.dat','w');
sfids = fopen('sspecial.dat','w');
sfidf = fopen('sfake.dat','w');
sfidd = fopen('sdisk.dat','w');
sfidr = fopen('srotate.dat','w');
sfidx = fopen('stranx.dat','w');
sfidy = fopen('strany.dat','w');
%Builds the square mine image, it has to be
%larger then 65x65 so that I can filter it
fake=zeros(68);
fake=fake+6979;
x=23:47;
y=23:47;
fake(x,y)=fake(x,y)+3100;
%Loads the 65x65 image sp.dat load sp.dat
%Creates a round mine image, it also
%has to be larger then 65x65 so that I can filter it y=disk(68,34,34,12);
faked=6797+(y*12);
%Converts the sp.dat input to a 65x65 matrix
%also creates the 90 deg rotated image
for k=1:4225;
x=sp(k,1);
y=sp(k,2);
sps(x,y)=sp(k,3);
spr(y,x)=sp(k,3);
end;
%Plots the original image and the rotated image subplot(3,2,1),contour (sps); subplot
(3,2,2),contour (spr);
 %This is the spatial lowpass matrix l=[1,1,1,1 1,1,1,1 1,1,1,1 1,1,1,1];
%This is where the two fake images are filtered
lfake=conv2(fake,l,'valid')/9;
```

```
lfaked=conv2(faked,l,'valid')/9;
%Plots the two filtered images
subplot (3,2,6),contour (lfaked);
subplot(3,2,5),contour(lfake);
%Takes the 2D ff transform
flfake=fft2(lfake);
flfaked=fft2(lfaked);
fsps=fft2(sps);
fspr=fft2(spr);
%Calculates the difference matrixs for the rotated,
%disk and square images compared to the original
diff=fspr-fsps;
fddiff=flfaked-fsps;
fdiff=flfake-fsps;
%Prints out the rotated difference (sqrt of %the sum of the squared diff)
rotated=abs(sqrt(sum(sum(diff^2))))
%Builds the x and y shifted images
x=1:60;
y=1:65;
ssps(x+5,y)=sps(x,y);
sssps(y,x+5)=sps(y,x);
x=1:5;
ssps(x,y)=sps(x+60,y);
sssps(y,x)=sps(y,x+60);
%Plots the shifted images
subplot (3,2,3),contour (ssps);
subplot(3,2,4),contour(sssps);
%Takes the 2D ff transfroms of the shifted images
fssps=fft2(ssps);
fsssps=fft2(sssps);
%Calculated the difference matrixs for the shifted images
sdiff=fssps-fsps;
ssdiff=fsssps-fsps;
%Prints out the translated, square and disk differences (sqrt of %the sum of the squared
diff) tranlatedx=abs(sqrt(sum(sum(sdiff^2))))
translatedy=abs(sqrt(sum(sum(ssdiff^2))))
square=abs(sqrt(sum(sum(fdiff^2))))
circle=abs(sqrt(sum(sum(fddiff^2))))
%prints out the sum of the differences
rot=abs(sum(sum(diff)))
transx=abs(sum(sum(sdiff)))
transy=abs(sum(sum(ssdiff)))
squ=abs(sum(sum(fdiff)))
cir=abs(sum(sum(fddiff)))
%Writes the files in a format for surfer to plot
```

```
for x=1:65;
for y=1:65;
fprintf(fidf,'%2d %2d %12d\n',x,y,lfake(x,y));
fprintf(fidd,'%2d %2d %12d\n',x,y,lfaked(x,y));
fprintf(fidr,'%2d %2d %12d\n',x,y,spr(x,y));
fprintf(fidx,'%2d %2d %12d\n',x,y,ssps(x,y));
fprintf(fidy,'%2d %2d %12d\n',x,y,sssps(x,y));
end
end
figure sfssps=fftshift(fssps);
sfsps=fftshift(fsps);
sfspr=fftshift(fspr);
sfsssps=fftshift(fsssps);
sflfake=fftshift(flfake);
sflfaked=fftshift(flfaked);
subplot(3,2,1),contour(log(abs(abs(sfsps))));
subplot(3,2,2),contour(log(abs(abs(sfspr))));
subplot(3,2,3),contour(log(abs(abs(sfssps))));
subplot(3,2,4),contour(log(abs(abs(sfsssps))));
subplot(3,2,5),contour(log(abs(abs(sflfake))));
subplot(3,2,6),contour(log(abs(abs(sflfaked))));
for x=1:65;
for y=1:65;
fprintf(sfidf,'%2d %2d %12d\n',x,y,log(abs(abs(sflfake(x,y)))));
fprintf(sfidd,'%2d %2d %12d\n',x,y,log(abs(abs(sflfaked(x,y)))));
fprintf(sfids,'%2d %2d %12d\n',x,y,log(abs(abs(sfsps(x,y)))));
fprintf(sfidr,'%2d %2d %12d\n',x,y,log(abs(abs(sfspr(x,y)))));
fprintf(sfidx,'%2d %2d %12d\n',x,y,log(abs(abs(sfssps(x,y)))));
fprintf(sfidy,'%2d %2d %12d\n',x,y,log(abs(abs(sfsssps(x,y)))));
end
end
```

LIST OF REFERENCES

[1] Campbell, J. and Jacobs, A., "Detection of buried landmines by Compton backscatter imaging," *Nuclear Science and Engineering*, 110, pp. 417-424, 1992.

[2] Watanabe, Y., Monroe, J., Keshavmurthy, S., Jacobs, A., Dugan, E., "Computational methods for shape restoration of buried objects in Compton backscatter imaging," *Nuclear Science and Engineering*, 122, pp. 55-67, 1996.

[3] Wehlburg, J., Keshavmurthy, S., Watanabe, Y., Dugan, E., Jacobs, A., "Image restoration techniques using Compton backscatter imaging for detection of buried landmines," SPIE Proceeding on *Detection technology for mine and minelike targets*, 2496, pp. 336-347, 1995.

[4] Wehlburg, J., Keshavmurthy, S., Dugan, E., Jacobs, A., "Experimental measurement of noise removal techniques for Compton backscatter imaging systems as applied to the detection of landmines," SPIE Proceeding on *Detection and remediation technologies for mine and minelike targets*, 2765, pp. 502-511, 1996.

[5] Keshavmurthy, S., Dugan, E., Wehlburg, J., Jacobs, A., "Analytical studies of a backscatter x-ray imaging landmine detection system," SPIE Proceeding on *Detection and remediation technologies for mine and minelike targets*, 2765, pp. 512-523, 1996.

[6] Evans, R., The Atomic Nucleus, Krieger Publishing Company, Malabar (FL), 1985.

[7] Harding, G., Kosanetsky, J, "Scatter x-ray beam nondestructive testing," *Nuclear Instrumentation and Methods in Physics Research*, A280, pp. 517-528, 1989.

[8] Herr, M., McInernney, J., Lamser, D., Copenhaver, G., " A flying spot x-ray system for Compton backscatter imaging," *IEEE transactions on Medical Imaging*, 13(5), 461-469, 1994.

[9] Harrison, M., The Effects of Detector Height Variation on Backscatter Imaging of Buried Landmines, Masters Thesis, University of Florida, 1989.

[10] Attix, F., Introduction to Radiological Physics and Radiation Dosimetry, John Wiley &Sons, New York, 1986.

[11] Keshavmurthy, S., Development of a Lateral Migration Backscatter Radiography and Associated Image Enhancement Algorithms, Doctor of Philosophy Thesis, University of Florida, 1996.

[12] General Electric Corporation, Maxitron 300 X-ray Therapy Unit Operation, Maintenance, General Electric Directions No. 12338C, General Electric X-ray Department, Milwaukee, WI, 1960.

[13] Moss, D., An X ray Backscatter Imaging System: Hardware and Software Development, Masters Thesis, University of Florida, 1987.

[14] Monroe, J., The Development, Implementation, and Testing of an X ray Backscatter Imaging System for the Detection of Buried Landmines, Engineer Thesis, University of Florida, 1993.

[15] Campbell, J., Landmine Detection by Scatter Radiation Radiography, Doctor of Philosophy Thesis, University of Florida, 1987.

[16] Monroe, J., Mine Imaging with Backscattered Radiation using Sampling of a Current Mode Signal, Masters Project, University of Florida, 1990.

[17] Hanselman, D., Littlefield, B., The MATLAB: Version 4.0: User's guide, Mathworks Inc., Prentice-Hall, Englewood Cliffs, NJ, 1995.

BIOGRAPHICAL SKETCH

Joseph C. Wehlburg is a native of Gainesville, Florida, born on August 14, 1968. He obtained his bachelor degree in nuclear engineering from the University of Florida in the Fall of 1992. He married Christine Marie Polesnak on November 13, 1993. On December 14, 1994, their daughter, Rachel Susan-Marie Wehlburg, came into this world at a whopping 11 lbs 3 oz, by natural childbirth. He received his Master of Engineering in nuclear engineering from the University of Florida shortly thereafter in December of 1994 and will be completing his Ph.D. in nuclear engineering with a minor in computer and information science and engineering in May of 1997. He will be going on to work for Sandia National Labs.

I certify that I have read this study and that in my opinion it conforms to acceptable standards of scholarly presentation and is fully adequate, in scope and quality, as a dissertation for the degree of Doctor of Philosophy.

Alan M. Jacobs

Alan M. Jacobs, Chairman
Professor of Nuclear and
Radiological Engineering

I certify that I have read this study and that in my opinion it conforms to acceptable standards of scholarly presentation and is fully adequate, in scope and quality, as a dissertation for the degree of Doctor of Philosophy.

Edward T Dugan

Edward T. Dugan
Associate Professor of
Nuclear and Radiological
Engineering

I certify that I have read this study and that in my opinion it conforms to acceptable standards of scholarly presentation and is fully adequate, in scope and quality, as a dissertation for the degree of Doctor of Philosophy.

Samim Anghaie

Samim Anghaie
Professor of Nuclear and
Radiological Engineering

I certify that I have read this study and that in my opinion it conforms to acceptable standards of scholarly presentation and is fully adequate, in scope and quality, as a dissertation for the degree of Doctor of Philosophy.

Andrew Laine

Andrew F. Laine
Associate Professor of
Computer and Information
Science and Engineering

I certify that I have read this study and that in my opinion it conforms to acceptable standards of scholarly presentation and is fully adequate, in scope and quality, as a dissertation for the degree of Doctor of Philosophy.

Martin T. Vala

Martin T. Vala
Professor of Chemistry

This dissertation was submitted to the Graduate Faculty of the College of Engineering and to the Graduate School and was accepted as partial fulfillment of the requirements for the degree of Doctor of Philosophy.

May, 1997

Winfred M. Phillips
Dean, College of Engineering

Karen A. Holbrook
Dean, Graduate School